Thesis for the degree of Doctor of Philosophy

High-redshift active galactic nuclei and their environment

OLIMPIA JUDIT FOGASY

CHALMERS

Department of Space, Earth and Environment
CHALMERS UNIVERSITY OF TECHNOLOGY
Gothenburg, Sweden 2020

High-redshift active galactic nuclei and their environment
OLIMPIA JUDIT FOGASY

ISBN: 978-91-7905-326-0
Doktorsavhandlingar vid Chalmers tekniska högskola
Ny series Nr 4793
ISSN 0346-718X

Astronomy & Plasma Physics, Extragalactic Astronomy
Department of Space, Earth and Environment
Chalmers University of Technology
SE–412 96 Gothenburg, Sweden
Phone: +46 (0)31–772 1000

Contact information:
Judit Fogasy
Onsala Space Observatory
Chalmers University of Technology
SE–439 92 Onsala, Sweden

Phone: +46 (0)31–772 5543
Fax: +46 (0)31–772 5590
Email: judit.fogasy@chalmers.se

Cover image:
The Hubble eXtreme Deep Field image combines Hubble observations taken over several years of a small patch of sky in the constellation of Fornax.
Image credit: NASA, ESA, G. Illingworth, D. Magee, and P. Oesch (University of California, Santa Cruz), R. Bouwens (Leiden University), and the HUDF09 Team

Printed by Chalmers Reproservice
Chalmers University of Technology
Gothenburg, Sweden 2020

High-redshift active galactic nuclei and their environment

OLIMPIA JUDIT FOGASY
Department of Space, Earth and Environment
Chalmers University of Technology

Abstract

In order to understand the formation and evolution of local massive galaxies and to reveal the processes that engineered the tight correlations found between their supermassive black hole (SMBH) mass and bulge mass or velocity dispersion, the study of powerful, high-redshift active galactic nuclei (AGNs) and their environment is crucial. AGNs are luminous targets providing important clues to galaxy evolution, as their central SMBH is growing at high rates, which opens the opportunity to unfold how the growth of the black hole influences the growth of its host galaxy. Moreover, powerful high-z AGNs are hosted by massive galaxies and likely trace protoclusters, where the progenitors of present-day massive galaxies reside. Observations of high-z quasars and radio galaxies suggest that these AGNs live in overdense environment surrounded by star-forming Lyα-emitters and submillimetre galaxies. At smaller scales several high-z quasars and radio galaxies have gas-rich and/or star-forming companion galaxies.

The aim of this thesis is to study the environment of high-z quasars and radio galaxies through submillimetre and CO spectral line observations and to contribute to the effort of uncovering the underlying processes that shape the evolution of massive galaxies. The thesis focuses on three case studies of high-z AGN–companion galaxy systems at $z = 2 - 3$. These were selected based on the AGN host galaxy appearing as gas-poor, while the companion galaxy being very gas-rich. However, sensitive observations with the Atacama Large Millimeter/submillimeter Array and the Karl G. Jansky Very Large Array, tracing CO line emission and dust continuum emission, revealed that a significant amount of molecular gas and dust emission is associated with the host galaxies of the AGNs. My results highlight the importance of sensitive and high-resolution observations and demonstrate that high-z AGN systems are more complex and diverse, than it is implied by theoretical studies.

Keywords: galaxies: evolution – galaxies: high-redshift – galaxies: active – galaxies: Starburst – – Submillimeter: galaxies

Research contributions

This thesis is based on the following appended papers:

- J. Fogasy, K. K. Knudsen, C. D. P. Lagos, G. Drouart, V. Gonzalez-Perez:
  On the frequency of star-forming galaxies in the vicinity of powerful AGNs: the case of SMM J04135+10277
  Astronomy & Astrophysics, 597, A123, 2017

- J. Fogasy, K. K. Knudsen, C. D. P. Lagos, G. Drouart, L. Fan:
  SMM J04135+10277: A distant QSO–starburst system caught by ALMA
  Monthly Notices of the Royal Astronomical Society, Volume 493, Issue 3, p.3744-3756, 2020

- J. Fogasy, K. K. Knudsen, G. Drouart, B. Gullberg:
  ALMA detects molecular gas in the halo of the powerful radio galaxy TXS 0828+193
  Monthly Notices of the Royal Astronomical Society, submitted (2020)

- J. Fogasy, K. K. Knudsen, E. Varenius:
  VLA detects CO(1–0) emission in the $z = 3.65$ quasar SDSS 160705+533558
  Manuscript intended for submission to Astronomy & Astrophysics

I also participated in the following papers not included in the thesis:

- S. Frey, Z. Paragi, O. J. Fogasy, L. I. Gurvits:
  The first estimate of radio jet proper motion at $z > 5$
  Monthly Notices of the Royal Astronomical Society, 446, 3, p.2921-2928, 2015

- L. Fan, K. K. Knudsen, G. Drouart, J. Fogasy
  ALMA Detections of CO Emission in the Most Luminous, Heavily Dust-obscured Quasars at $z > 3$
  The Astrophysical Journal Letters, 856, 1, L5, 2018.

Acknowledgements

I would like to thank my supervisor Kirsten K. Knudsen for her help and encouragement throughout my doctoral studies. I am very grateful that I had the opportunity to work in her research group. I am also grateful for the scientific discussions with Susanne Aalto, Guillaume Drouart, John Black, and Alessandro Romeo. I am thankful for Sabine König and Eskil Varenius for their help and expertise on interferometric data reduction. In addition, I feel grateful for the inspiring and supporting environment at the Onsala Space Observatory and Chalmers, and for all the wonderful current and former PhD students and postdocs I have met here in the past years. A special thanks goes to Suzy Jones, for being a great friend and Flora Stanley, for being a supportive office mate. Finally, I would like to thank my family and friends for supporting me, my mum for her pep talks, my husband, Tamás for his love and my little son, Ervin, whose existence inspires and motivates me the most to achieve my goals.

Judit

Contents

Chapter 1

Introduction

One of the greatest and most important discoveries in the field of astronomy is the realization that the Milky Way is just one of billions of galaxies in the Universe. Since then, millions of galaxies have been observed, studied and categorized, which revealed that galaxies come in many different colours and sizes and they undergo cosmic evolution.

Studies of the Milky Way and nearby galaxies helped to reveal the basic building blocks of galaxies and understand the underlying physics that connects them. In the most general sense a galaxy is a gravitationally bound system of stars. The regions between stars contain gas and dust, jointly referred to as the interstellar medium (ISM). In addition to stars and the ISM, galaxies have two other components, which are more difficult to observe. Stellar kinematic observations and dynamical models revealed that our Galaxy harbours a supermassive black hole (SMBH, $M_{\rm BH} \sim 10^6 M_\odot$) in its center (e.g. Eckart & Genzel 1996; Ghez et al. 1998; Genzel et al. 2000). Extensive studies of galaxies found similar conclusions and today it is widely accepted that every massive galaxy contains a supermassive black hole (e.g. Kormendy & Richstone 1995; Richstone et al. 1998; Magorrian et al. 1998; Kormendy & Ho 2013). If the SMBH is actively growing by accreting gas from its surrounding, the central region of the galaxy is called active galactic nucleus (AGN). The last component and maybe the most important is dark matter. The existence of dark matter is predicted by the Standard Model of Cosmology and it accounts for $\sim 85\%$ of the total mass in the Universe. Although dark matter has not been observed directly, evidence for its existence comes from e.g. observations of galaxy kinematics and dynamics (galaxy rotation curve and velocity dispersion measurements), gravitational mass measurements of galaxy clusters, gravitational lensing, fluctuations in the cosmic microwave background (CMB).

Galaxies in the local Universe show bimodality regarding their colour and morphology. The two main classes of galaxies are spiral galaxies (late type), which are blue and star-forming, and elliptical galaxies (early type), which are red and

passive in terms of star formation. The different colours of spiral and elliptical galaxies indicate different stellar populations: spiral galaxies have very mixed stellar populations, containing both young, hot, therefore blue Population I stars and old Populations II stars, while ellipticals have mostly old, cooler stars, and therefore they appear red. The shape of elliptical galaxies is ellipsoidal, with smooth brightness profiles. Based on the shape of their isophotes, they can be disky or boxy ellipticals. Boxy ellipticals represent the highest mass galaxies in the Universe and contain large amount of X-ray gas in their halo, while disky ellipticals tend to be smaller in size and lack the hot X-ray gas component (e.g. Cappellari et al. 2013; Kormendy & Ho 2013). Spiral galaxies have more structure, they contain a thin rotating disk, a central, dense region of stars called bulge and in some cases bars. Bulges can be divided into two groups: classical bulges are much rounder than their disks, their Sérsic indices are $n \geq 2$; pseudo-bulges have more disky-like morphology, their Sérsic indices are $n \leq 2$ (Renzini 1999; Kormendy & Kennicutt 2004).

Observations of local, massive elliptical galaxies revealed tight correlations between the mass ($M_{\rm bulge}$) or velocity dispersion (σ) of the host galaxy and the mass of its supermassive black hole ($M_{\rm BH}$) (e.g. Magorrian et al. 1998; Gebhardt et al. 2000; Merritt & Ferrarese 2001; Tremaine et al. 2002; Marconi & Hunt 2003; Häring & Rix 2004; McConnell & Ma 2013). Equation 1.1 shows the above correlations for ellipticals and classical bulges based on the compilation of extensive samples (Kormendy & Ho 2013):

$$\begin{aligned}
\frac{M_{\rm BH}}{10^9 {\rm M}_\odot} &= 0.542^{+0.069}_{-0.061}\left(\frac{L_{\rm K,bulge}}{10^{11}{\rm L}_{\rm K\odot}}\right)^{1.21\pm0.09}, \\
\frac{M_{\rm BH}}{10^9 {\rm M}_\odot} &= 0.309^{+0.037}_{-0.033}\left(\frac{\sigma}{200{\rm kms}^{-1}}\right)^{4.38\pm0.29}, \\
\frac{M_{\rm BH}}{10^9 {\rm M}_\odot} &= 0.49^{+0.06}_{-0.05}\left(\frac{M_{\rm bulge}}{10^{11}{\rm M}_\odot}\right)^{1.16\pm0.08},
\end{aligned} \tag{1.1}$$

An interesting aspect of these correlations is that they only hold for elliptical galaxies and galaxies with classical bulges (Kormendy et al. 2009). The $M_{\rm BH}$ does not correlate with so-called pseudo-bulges or disk galaxies, nor with galaxy disks. This suggests that SMBHs in disk galaxies and classical bulges/ellipticals might grow via different feeding mechanisms. During major galaxy mergers all conditions are met so that global feeding can occur, which likely leads to the formation of classical bulges and ellipticals. On the other hand, SMBHs in disk galaxies are fed via secular, internal processes which cannot engineer a tight correlation between the SMBHs and their host galaxies.

Besides the tight correlations between $M_{\rm BH} - M_{\rm bulge}$ and $M_{\rm BH} - \sigma$, there are other signs suggesting that SMBHs and ellipticals/bulges evolve together. For

example, the histories of the cosmic star formation rate and black hole growth are similar, a significant fraction of starburst galaxies contain buried AGN and the host galaxies of luminous AGNs tend to be star-forming. This implies that AGN activity and star formation is linked. Based on the Soltan's argument, most of the SMBH mass must have been grown while the galaxy hosted an AGN, which means that SMBHs in local galaxies are the final products of high-redshift AGN episodes (Soltan 1982). Thus, beyond major merger events, AGN feedback may play an important role in establishing the observed correlations.

The aim of this thesis

How do galaxies grow and evolve? What is the origin of the local bimodal distribution of galaxies regarding their colour, morphology, star formation? What processes engineer the tight correlations found between the SMBH mass and the bulge mass/velocity dispersion of local massive galaxies? When are these correlations established? How does the host galaxy know what happens near the SMBH and vice versa? What are the processes that trigger the growth of the SMBH and star formation in the host? Where and how did the stellar mass of local massive ellipticals form and assemble: during starburst events triggered by galaxy interactions, by mergers of gas-rich progenitors or in close star-forming companion galaxies of high-redshift AGNs, which eventually merged? What role does the environment play in galaxy formation?

These questions have inspired many scientists in the past few decades and though a significant amount of progress has been made, many of the fundamental questions still lack answers. One way to start is to study high-z luminous AGNs and their environment. As powerful AGNs are hosted by massive galaxies, they likely trace overdense environments or protoclusters, where the progenitors of present day massive ellipticals reside. Moreover, AGNs are valuable and interesting targets, since their SMBH is feeding and growing, which opens the opportunity to unfold how the growth of the black hole influences the growth of its host galaxy.

The aim of this thesis is to study the environment of high-z quasars and radio galaxies, the possible progenitors of local massive galaxies. Chapter 2 describes the scene of high-redshift studies including the cosmic evolution of galaxies, the types of distant galaxies and their ISM. Chapter 3 summarises the current AGN classification scheme and unification theory, discusses the role of AGN feedback in the evolution of massive galaxies and summarises the results of recent AGN environment studies both on large and small scales. Chapter 4 gives a short introduction to radio astronomy and the observing facilities used in the appended papers. Chapter 5 gives an introduction to the appended papers, including the tools used in the data analysis. Chapter 6 summarises the appended papers. Chapter 7 gives an outlook and discusses future prospects.

Chapter 2

Distant galaxies

2.1 Cosmic evolution of galaxies

The bimodality of present-day[1] galaxies may arise from different evolutionary paths. In order to investigate how they formed, grew and reached their current appearance, one has to look at the various ways a galaxy can grow. According to the currently accepted cosmological model, the Λ Cold Dark Matter model (ΛCDM), structure formation started from primordial density fluctuations followed by gravitational collapse of dark matter, leading to the formation of dark matter haloes (e.g. White & Rees 1978; Blumenthal et al. 1984; Davis et al. 1985). As the virial equilibrium is reached in the halo, the collapse of dark matter stops. Haloes then grow hierarchically, via merging with other virialized haloes. The deep potential well of dark matter haloes causes the baryonic matter to infall, collapse, radiate away its binding energy and form smaller structures, such as stars and galaxies.

There are two possible ways to supply a galaxy with gas and grow its stellar mass: merger events and gas accretion from the intergalactic medium (IGM). Depending on the mass ratio of the merging galaxies, we distinguish between major (ratio>1:3), minor (<1:10) and intermediate (1:3–1:10) merger events (Shlosman 2013). If the merging galaxies are gas-rich, the merger event is dissipative and is often referred to as "wet" merger. In case of merging of gas-poor galaxies, the merger is "dry" and dissipationless. In general, gas-rich mergers were dominant at high-z, while dissipationless merger events are more frequent at lower redshifts (e.g. Faber et al. 2007; Lin et al. 2010).

Major gas-rich mergers are proposed to be responsible for triggering starburst events, driving gas into the central regions of the galaxy and fuelling the SMBH, which then appears as an AGN (e.g. Sanders & Mirabel 1996; Hopkins et al. 2006,

[1]The age of the Universe is ~ 13.8 Gyr. Adopting WMAP7 cosmology with $H_0 = 70.4$ km s^{-1}Mpc^{-1}, $\Omega_{\rm m} = 0.272$ and $\Omega_\Lambda = 0.728$, at redshifts $z = 3$ and $z = 2$ the Universe is ~ 2.2 Gyr and ~ 3.4 Gyr old, respectively.

2008). As the AGN becomes more powerful it influences its host galaxy through AGN feedback, in form of winds, powerful outflows, and radio jets, which likely suppress the star formation. While the merger scenario is appealing, observations of high-z star-forming galaxies and AGN studies indicate that mergers are not the only and dominant way of galaxy growth and AGN triggering.

Galaxies can accrete gas from the IGM. Based on the early studies of galaxy formation, which assumed spherical symmetry, gas falling into the potential well of a dark matter halo is shock-heated to the virial temperature of the halo ($T_{\rm vir} \sim 10^6\,{\rm K}$) and reaches pressure supported quasi-static equilibrium with dark matter. By radiating away its thermal energy the gas can cool in the inner regions of the halo and settle into a rotationally supported disk, where it can form stars (e.g. Rees & Ostriker 1977; Silk 1977; Fall & Efstathiou 1980; White & Frenk 1991).

In contrast to early models of galaxy formation, hydrodynamical numerical simulations, such as the Virgo Consortium Millenium Simulation and the Illustris Simulation, show different geometry than spherical: the large scale structure of the Universe contains filaments and sheets, separated by empty spaces, voids (e.g. Springel et al. 2005; Vogelsberger et al. 2014). Galaxies primarily form along the filaments, the most massive galaxies at the intersections of filaments. Simulations also reveal that a large fraction of the accreted gas is never shock-heated to $T_{\rm vir}$ but radiates its gravitational energy from $T \leq 10^5\,{\rm K}$. This mode of accretion is called "cold mode" , while the conventional accretion is called as "hot mode" (Katz et al. 2003; Kereš et al. 2005). Galaxies fed along filaments can grow through cold mode accretion in the form of cold streams (e.g. Dekel et al. 2009b; Fumagalli et al. 2011; Rosdahl & Blaizot 2012). Moreover, both accretion modes can coexist, especially at high-z, where dense, cold filaments may penetrate through the hot haloes of massive galaxies (Kereš et al. 2005; Dekel et al. 2009a).

Direct detection of the filamentary structure of the cosmic web is challenging but in the recent years significant effort has been put into observing the gaseous filaments. One way to trace neutral hydrogen in the IGM is to use absorption spectroscopy on background sources (e.g. quasars), where Lyman-α absorption lines (Ly-α forest) indicate the presence of HI along the line of sight (e.g. Caucci et al. 2008; Stark et al. 2015; Lee et al. 2016; Lee & White 2016). Other methods include searching for Lyman-α emission around star-forming galaxies and AGN or using Lyman-α emitting galaxies (LAEs) as tracers (e.g. Cantalupo et al. 2005, 2014; Martin et al. 2015; Swinbank et al. 2015; Borisova et al. 2016; Vernet et al. 2017; Umehata et al. 2019).

The mode of gas accretion depends on the redshift, the halo mass and the environment (e.g. Kereš et al. 2005; Dekel & Birnboim 2006; van de Voort et al. 2011b, 2017). At higher redshifts ($z > 3$) the density of the gas is higher, the radiative cooling is more efficient, hence cold accretion is more dominant, whereas at low redshift hot mode accretion takes over. Higher mass haloes ($M_{\rm halo} \geq 10^{11}\,{\rm M}_\odot$) have higher virial temperatures and therefore longer cooling times and the gas is

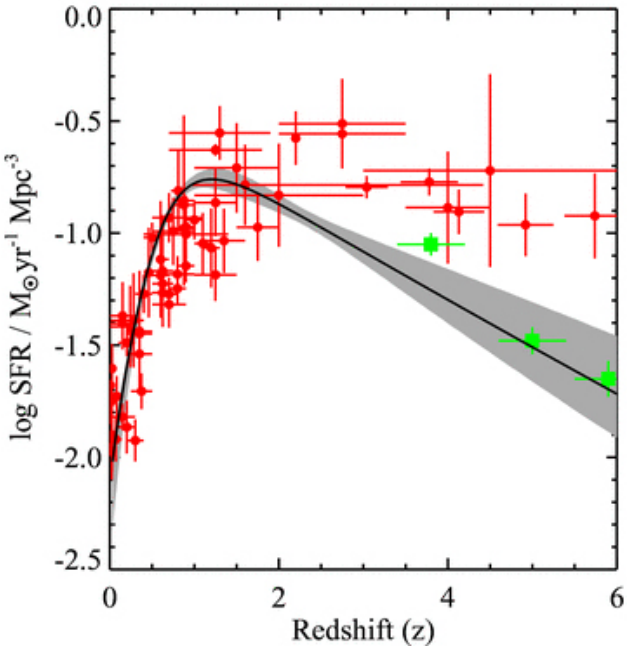

Figure 2.1: Redshift evolution of the black hole accretion rate (solid line; grey shaded area indicates 1σ uncertainty of the model) and the cosmic star formation rate (circles and squares from Hopkins 2004; Bouwens et al. 2007, respectively). The black hole accretion rate is scaled up by a factor of 5000. The figure is adapted from Aird et al. (2010, Fig.13).

accreted in hot mode. Looking at the environment cold accretion dominates in less dense environment and hot mode accretion dominates in group and cluster environments at low redshift.

By distinguishing between accretion onto haloes and galaxies, the specific accretion rate of haloes increases with halo mass, while the accretion rate onto galaxies drops at $M_{\rm halo} \gg 10^{12}\,{\rm M}_{\odot}$ (e.g. van de Voort et al. 2011b). Looking at the relative contribution of the two modes, the hot mode accreation onto haloes becomes more important at higher mass haloes ($M_{\rm halo} \geq 10^{11}\,{\rm M}_{\odot}$). However, the hot fraction of the gas accreted onto galaxies does not depend on the halo mass. Moreover, while the accretion onto haloes is insensitive to metal-line cooling and feedback from star formation and AGN, these processes affect the accretion onto galaxies, thus controlling their growth and evolution (e.g. van de Voort et al. 2011b).

Looking at the redshift evolution of the star formation rate density, it is clear that the Universe was much more active at higher-redshifts (Figure 2.1). The peak of the star formation rate density is around $z = 2 - 3$, which is followed by an exponential decline toward lower redshifts. At the peak, the star formation rate (SFR) was $\sim 10\times$ higher compared to its present day value (e.g. Madau &

Dickinson 2014). The evolution of the cosmic star formation rate is governed by the growth of dark matter haloes and the gas accretion mode. Based on numerical simulations, the decline of the global SFR might be the result of the drop of the global cold accretion mode onto haloes in addition to feedback processes (e.g. van de Voort et al. 2011a; Nelson et al. 2015; Aragon Calvo et al. 2019). While the hot mode accretion does not show such drop, a large fraction of the accreted gas has longer cooling time than the Hubble time, thus it cannot be accreted by the galaxies to feed star formation.

Both merger events and gas accretion from the IGM play an important role in galaxy evolution: gas-rich major mergers can induce vigorous starbursts and trigger luminous AGN, dissipationless dry mergers account for the formation of the most massive core-boxy ellipticals, while cold accretion supplies disk galaxies and lower luminosity AGN. Moreover, the two modes of gas accretion gives a plausible explanation why massive systems are passive, while lower mass galaxies, spirals have on-going star formation.

2.2 Molecular gas and dust

General references: Draine (2011); Carilli & Walter (2013)
The gas and dust commonly referred to as the interstellar medium are very important components of galaxies. Stars form from interstellar clouds and gas can provide fuel for the central supermassive black hole. Dust not only traces star-formation in otherwise obscured sources through its thermal emission but acts as a catalyst for molecular hydrogen formation. By studying these components in high-redshift sources we can learn about their evolution, i.e. how much gas is available for building new stars or to fuel an AGN, and learn about the physical conditions of their ISM.

Atomic and molecular hydrogen

The interstellar gas primarily consists of hydrogen and helium, while also contains heavier elements, so-called metals. The atomic hydrogen (HI) can be observed through the 21 cm (1420 MHz) hyperfine line, originating from the hyperfine splitting of the 1s electronic ground state of hydrogen. In the ground state of hydrogen, the electron and proton can be either parallel or anti-parallel, with the former being a higher energy state. When the spin of the electron flips to anti-parallel position a photon is emitted at 21 cm. As the energy difference between these two hyperfine levels is small, it is easily excited even by the CMB radiation. The 21 cm line is used to map the HI distribution of the Milky Way and other nearby galaxies and determine their HI mass, to constrain the galactic rotation curve and to measure the temperature of interstellar clouds.

At the sites of star-formation, in giant molecular clouds with densities of $n > 100\,\mathrm{cm}^{-3}$, most of the hydrogen is in molecular form (H_2). The dominant process to form H_2 is via grain catalysis. In this case dust grains provide the surface for HI atoms to get trapped and react to form H_2. Molecular hydrogen is destroyed via photodissociation by ultraviolet (UV) photons with energy of $11.2\,\mathrm{eV} < h\nu < 13.6\,\mathrm{eV}$. However, H_2 is protected by dust extinction and self-shielding at sufficiently high column densities ($N_{H_2} > 10^{15}\,\mathrm{cm}^{-2}$). This means that only a small fraction of the photons absorbed by H_2 leads to its dissociation.

Molecular hydrogen is very difficult to observe directly as it is a homonuclear molecule and therefore has no permanent electric dipole moment. Without electric dipole transitions all the low-energy transitions are quadrupole. These transitions require very large excitation temperatures (500 K for the $J = 2 \rightarrow 0$), have small transition probabilities and radiate very weakly. Moreover, as the rotational lines occur in the mid-infrared (MIR), their detection is challenging due to the limited atmospheric transition. Thus, even though H_2 is the most abundant molecule of the ISM and provides the raw material to form stars, we effectively cannot observe it in emission. Instead, we can use proxy molecules to indirectly detect H_2 and infer its mass.

Carbon monoxide as molecular gas tracer

The second most abundant molecule of the ISM is carbon monoxide (CO). CO is more massive than H_2 and its low-J rotational states have low excitation temperatures ($J = 1$ is only 5.5 K above the ground state). These properties and the fact that CO emission lines can be observed from the ground makes it the perfect molecular gas tracer. The most common isotopologue of CO is $^{12}C^{16}O$, which has high optical depth, making it easier to observe compared to other CO isotopologues, which are mostly optically thin (e.g. $^{13}C^{16}O$,$^{12}C^{18}O$).

CO can be excited through collisions with H_2 and He and through radiative absorption. In a thermalized system the relative level populations can be described by the Boltzmann-distribution,

$$\frac{n_\mathrm{u}}{n_\mathrm{l}} = \frac{g_\mathrm{u}}{g_\mathrm{l}} e^{-h\nu/kT_\mathrm{ex}}, \tag{2.1}$$

where n_u and n_u are the populations of the upper and lower level, g_u and g_u are statistical weights and T_ex is the excitation temperature. In this case the system is in local thermal equilibrium (LTE) and the excitation temperature is the same as the kinetic temperature of the gas. In a sub-thermal system the upper-J levels become underpopulated due to the imbalance of radiative decay and collisional excitation. As the collisional rate depends on the density of the gas, there is a critical density at which the rates of these two processes are the same:

$$n_\mathrm{crit} = \frac{A_\mathrm{ul}}{\gamma}, \tag{2.2}$$

where $A_{\rm ul} \propto \nu^3 \times \mu^2$ is the Einstein coefficient for spontaneous emission, which depends on the frequency ν and molecular dipole moment μ, and γ is the collision rate coefficient. The excitation of higher rotational levels requires higher energies, thus in order for the higher-J levels to be in LTE with low-J levels, higher critical densities and excitation temperatures are needed. For instance, the critical density for the CO($J = 1 \rightarrow 0$) transition is $n_{\rm crit} \sim 2.1 \times 10^3\,{\rm cm}^{-3}$, while for the CO($J = 8 \rightarrow 7$) transition it is $n_{\rm crit} \sim 6.4 \times 10^5\,{\rm cm}^{-3}$ (Carilli & Walter 2013). Thus, low-J lines trace the diffuse and extended molecular gas, while high-J lines are better proxies of the highly excited, denser component of the molecular gas.

The CO(1–0) transition at a rest-frequency of 115.271 GHz is commonly used to determine the molecular gas mass of galaxies. This line is optically thick and usually very bright, so it is observable even in distant galaxies. To convert the observed flux density of CO to molecular gas mass requires a conversion factor $\alpha_{\rm CO}$ ($\rm M_\odot$), which is the ratio of total mass to total CO line luminosity (Dickman et al. 1986; Solomon et al. 1987):

$$M_{\rm H_2} = \alpha_{\rm CO} L^{'}_{\rm CO}. \tag{2.3}$$

The total line luminosity can be expressed as

$$L^{'}_{\rm CO} = 3.25 \times 10^7\, S_{\rm CO}\Delta v\, \nu_{\rm obs}^{-2}\, D_L^2\, (1+z)^{-3}, \tag{2.4}$$

where $S_{\rm CO}\Delta v$ is the velocity integrated flux, $\nu_{\rm obs}$ is the observed frequency of the line in GHz and D_L is the luminosity distance in Mpc (Solomon et al. 1992). Since $L^{'}_{\rm CO}$ is proportional to the surface brightness temperature $T_{\rm b}$, the $L^{'}_{\rm CO}$ ratio of two lines originating from the same source gives the ratio of their intrinsic surface brightness temperatures. In the case of thermalized, optically thick emission both $L^{'}_{\rm CO}$ and $T_{\rm b}$ are independent of the rest frequency and J, e.g. $L^{'}_{\rm CO}(J = 3 \rightarrow 2) = L^{'}_{\rm CO}(J = 1 \rightarrow 0)$.

A conversion factor of $\alpha_{\rm CO} \sim 4\,{\rm M_\odot}\,({\rm K\,km\,s^{-1}\,pc^2})^{-1}$ is found in the Milky Way and for normal, star-forming spiral galaxies with close to solar metallicities, while a conversion factor of $\alpha_{\rm CO} \sim 0.8\,{\rm M_\odot}\,({\rm K\,km\,s^{-1}\,pc^2})^{-1}$ is used in the case of ultra-luminous infrared galaxies (Solomon & Barrett 1991; Downes & Solomon 1998). At high redshift a starburst value of $\alpha_{\rm CO} \sim 0.8 - 1\,{\rm M_\odot}\,({\rm K\,km\,s^{-1}\,pc^2})^{-1}$ is assumed for submillimetre galaxies, mergers and quasar host galaxies, and $\alpha_{\rm CO} \sim 4{\rm M_\odot}\,({\rm K\,km\,s^{-1}\,pc^2})^{-1}$ for colour-selected galaxies (e.g. Tacconi et al. 2008; Daddi et al. 2010; Genzel et al. 2010; Ivison et al. 2011). However, the conversion factor is not well-understood, and heavily depends on the physical properties of the gas, such as it metallicity, density and temperature (for a complete review see Bolatto et al. 2013).

In terms of galaxy formation and evolution it is important to describe how efficiently a galaxy can turn its gas into stars. According to the Schmidt-Kennicutt relation, often referred to as the star formation law, the gas surface density correlates with the surface density of star-formation (Schmidt 1959; Kennicutt 1998):

$$\Sigma_{\rm SFR} \sim \Sigma_{\rm gas}^{n}. \tag{2.5}$$

Follow-up studies revealed that in fact this relation holds for molecular hydrogen and not HI, even though HI is initially needed to form H_2 (e.g. Wong & Blitz 2002; Bigiel et al. 2008; Leroy et al. 2008; Schruba et al. 2011). At high-z there are several factors, which make it difficult to measure the star formation law, such as not having resolved CO observations or difficulties in determining the optical sizes, thus only global measurements are used. In addition, in the case of high-z galaxies typically higher-J CO lines are available, which need to be converted to CO(1–0) luminosities assuming certain line luminosity ratios to infer the mass of the molecular gas, and the conversion factor α itself is a source of uncertainty.

While CO can be successfully used in many cases to estimate the total molecular gas mass, some caution needs to be taken when interpreting such results. Given that H_2 is more self-shielding than CO, the relative amount of CO and H_2 can change significantly with changing physical conditions. At higher redshifts the temperature of the CMB is higher, which can impact on the excitation properties, particularly for the low-J transitions (da Cunha et al. 2013). In addition, non-detections of low-J CO lines do not necessarily imply that a galaxy is gas-poor, rather that the excitation conditions favour the excitation of the higher-J lines. Since the excitation and brightness of CO is nearly linearly related, hotter CO will emit a stronger line for the same amount of molecular gas.

In summary, by observing CO emission in high-z galaxies with high-resolution and sensitivity, we can get information about their molecular gas content and excitation conditions, obtain redshift information for dusty galaxies, test the star formation law and study galaxy kinematics.

Interstellar dust

Molecular gas clouds are mixed with dust, which can be used as a diagnostic tool to infer the physical conditions of gas and trace otherwise obscured star formation and black hole growth. Interstellar dust grains have complex morphology and structure. The size distribution of grains is broad from $0.001\,\mu$m to $0.2\,\mu$m, with most of the surface area being in small grains, while larger grains dominate the dust mass (Draine 2011). The composition of dust varies a lot but the main components are build up from the most abundant condensible elements, such as C, O, Mg, Si and Fe. These elements are underabundant in the gas phase and assumed to be incorporated in dust grains. The most common materials of dust are silicates, oxides of Si, Mg and Fe, carbin solids, hydrocarbons, carbides and metallic Fe.

Dust was discovered due to its obscuring and reddening effects on stellar light, known as extinction (absorption and scattering of light; Trumpler 1930). The

extinction A_λ at a given wavelength is defined by

$$A_\lambda = 2.5 \log_{10} \left(\frac{F_{\lambda,0}}{F_\lambda} \right), \tag{2.6}$$

where F_λ is the observed flux of a star and $F_{\lambda,0}$ is the flux of the star without the effect of extinction. The attenuation of starlight by dust has a strong wavelength dependence described by the extinction curve: blue/UV light is more attenuated by dust than red ligth, thus light reaching us from stars is "reddened". This has an impact on how we can observe star-formation in high-z galaxies. The steepness of the extinction curve is measured by R_V, a dimensionless ratio:

$$R_V = \frac{A_V}{A_B - A_V} = \frac{A_V}{E(B-V)}, \tag{2.7}$$

where A_V and A_B are extinctions measured in the 547.0 nm V-band and the 440.5 nm B-band, and $E(B-V)$ is the so-called colour excess. R_V varies with the sightline, from $R_V = 3.1$ in the diffuse ISM of the Milky Way, to $R_V \sim 4-6$ in very dense molecular gas (e.g. Savage & Mathis 1979; Cardelli et al. 1989).

Both the composition and size distribution of dust particles affect the wavelength dependence of the extinction. In the near-infrared (NIR) the extinction curve can be approximated by a power-law with $\propto \lambda^{-1.7}$. In the visible/near-UV bands the extinction varies as $\propto \lambda^{-1}$ and is caused by particles with sizes of $< 0.1\,\mu$m. The extinction curve has a characteristic bump at 217.5 nm, caused by dust rich in carbon. In tha far-UV extinction is increasing non-linearly caused by very small grains with sizes $< 0.01\,\mu$m. Besides the continous extinction there are two strong absorption features at $9.7\,\mu$m and $18\,\mu$m caused by silicates, a broad extinction feature at $3.4\,\mu$m due to C–H stretching mode of hydrocarbons, several weak and broad extinction features, known as the diffuse interstellar bands (DIBs), absorption features from ice and absorption features from polycyclic aromatic hydrocarbons (PAHs; Draine 2003).

As the interstellar gas is well-mixed with dust grains, the gas-to-dust ratio can be inferred by comparing the observed extinction and neutral hydrogen column density N_H (Bohlin et al. 1978; Rachford et al. 2009):

$$\frac{N_\mathrm{H}}{E(B-V)} = 5.8 \times 10^{21}\,\mathrm{H\,cm^{-2}\,mag^{-1}}. \tag{2.8}$$

In the Milky Way the average gas-to-dust mass ratio is in the order 100, while it varies with metallicity (Draine & Li 2007; Rémy-Ruyer et al. 2014; Li et al. 2019).

In addition to extinction, dust can be observed through interaction with starlight including reflection and polarization of light, via emission in infrared bands (PAH features) and via its thermal continuum emission at infrared (IR) and submillimetre (submm) wavelengths. The $3-15\,\mu$m spectral region has several emission

features resulting from vibrational transitions of PAH molecules. The thermal emission of dust is from radiative heating by optical and UV photons. Compared to other gas tracers dust has the advantage of emitting continuum emission, which is easier to observe than spectral lines in the case of high-z galaxies.

Modelling the thermal dust emission of galaxies is a difficult task, as there are several factors which need to be taken into account, such as the composition of dust, galaxy structure and orientation, optical depth, heating sources (Casey et al. 2014). To model the complex dust emission detailed radiative transfer models and empirical models/templates can be used (e.g. Silva et al. 1998; Chary & Elbaz 2001; Dale et al. 2001; Zubko et al. 2004; Siebenmorgen & Krügel 2007; Draine & Li 2007). In addition, the dust emission of galaxies can be approximated by the combination of a single temperature modified blackbody function $S_\nu \propto (1 - e^{-\tau(\nu)})B_\nu(T)$ and a power law function $S_\nu \propto \nu^\alpha$, where $\tau(\nu) = (\nu/\nu_0)^\beta$, β is the spectral emissivity index, ν_0 is the frequency where the optical depth $\tau = 1$, and α is the the slope of the MIR power-law component (Casey et al. 2014). The modified blackbody nicely describes the dust emission spectrum at longer wavelengths ($\lambda > 50\mu$m), while the excess dust emission in the MIR, originating from hotter dust components, is better fitted with a power law. An interesting feature of the dust emission is that the majority of the total IR emission is dominated by the cold dust component, even though the hot dust component consists of several subcomponents.

2.3 High-redshift galaxies

Over the past decades several techniques have been developed to identify high-redshift galaxies, which is necessary to get an unbiased picture of high-z galaxy populations and their properties (e.g. stellar mass, star formation rate) and understand their formation and evolution. Based on different selection criteria we can trace different high-z galaxy populations, such as star-forming Lyman-α emitters (LAEs), Lyman-break (LBGs) and BzK galaxies, extreme starburst galaxies like dusty star-forming galaxies (DSFGs) and submillimetre galaxies (SMGs), and massive galaxies, like extremely red objects (EROs) and distant red galaxies (DRGs). Some of these represent separate classes of galaxies, while others represent different evolutionary phases. While there are several selection methods, below I summarise some of the most well-known ones.

Lyman-α emitters and Lyman-break galaxies

The Lyman-α emission line of HI is produced by the spontaneous decay from the first excited state to the ground state ($n = 2 \rightarrow 1$, where n is the principle quantum number) at a wavelength of 121.56 nm. LAEs are high-z star-forming galaxies, and are typically found by narrow-band filter observations or spectroscopic techniques.

LBGs are selected by the Lyman-break technique, which enables us to detect these galaxies in the optical regime (e.g. Partridge & Peebles 1967; Steidel et al. 1995). As young stars emit mostly UV light and photons with energies higher than the ionization energy of hydrogen, they are easily absorbed by neutral gas around star-forming regions. As a result a break can be observed in the spectral energy distribution (SED) of the galaxy at 91.2 nm rest-frame wavelength. In the case of high-z galaxies ($z \gtrsim 2.5$) this break will be redshifted to the optical band, thus can be used as a tracer of star-forming, distant galaxies.

BzK galaxies

The BzK criteria selects both star-forming and passively evolving galaxies at redshifts of $1.4 < z < 2.5$ based on two-colour criteria using the B, z and K photometric bands (Daddi et al. 2004). BzK galaxies can be identified by the following criteria:

$$BzK = (z - K)_{\mathrm{AB}} - (B - z)_{\mathrm{AB}},$$

where $BzK \geq -0.2$ selects star-forming and $BzK < -0.2 \cap (z - K)_{\mathrm{AB}} > 2.5$ selects passive galaxies at $z > 1.4$. Compared to UV selected galaxies at $z \sim 2$, BzK galaxies have higher reddening and star formation rate. Their redshift distribution and mass is similar to that of SMGs but the later have higher SFR, while BzK galaxies have higher space density.

Distant red galaxies and extremely red objects

In the case of very red galaxies, either because of dust reddening or containing old stellar populations, NIR imaging can be used to select high-z galaxies via the rest-frame Balmer-break and the 400 nm-break, which is due to metal line absorption in the atmospheres of old stars. DRGs can be identified at redshifts $2 < z < 4$ using the J and K band with the following criteria in the Vega photometric system: $J - K > 2.3$ (e.g. Franx et al. 2003).

EROs are also selected according to their very red optical to NIR colours and represent both star-forming systems and old passively evolving galaxies. EROs are mostly lower redshift sources ($z \sim 1$). The selection criteria is based on R and B bands: $R - K \gtrsim 5$ (Elston et al. 1988).

Dusty star-forming galaxies and submillimetre galaxies

The term DSFG covers a diverse selection of galaxies, which contain a substantial amounts of dust and are significantly obscured at UV-optical wavelengths but bright at IR and submm/mm wavelengths (e.g. Casey et al. 2014). The advantage of submm observations is the large negative K-correction as they sample the Rayleigh-Jeans regime of the SED, which is a strongly increasing function

of the frequency. Thus high-z galaxies have very similar brightness at submm wavelengths from $z = 1 - 8$ (e.g. Casey et al. 2014).

SMGs are a subset of DSFGs. SMGs are heavily dust-obscured, high-redshift ($z \gtrsim 2$) starburst galaxies (SFR $\gtrsim 1000\,\mathrm{M}_\odot\,\mathrm{yr}^{-1}$), bright at submm/mm wavelengths due to thermal dust emission. The dust emission is well-described by a modified blackbody spectrum with a peak close to $100\,\mu$m (Pope et al. 2006). SMGs were originally selected from the $850\,\mu$m maps of the Submillimetre Common-User Bolometer Array (SCUBA) and from 1.2 mm maps of the Max Planck Millimetre Bolometer Array (MAMBO; Smail et al. e.g 1997; Hughes et al. e.g 1998; Blain et al. e.g 2002; Dannerbauer et al. e.g 2004).

Chapter 3

Active galactic nuclei and their environment

Active galactic nuclei are the most powerful objects in the Universe, they release enormous amount of energy ($10^{42} - 10^{47}$ erg s^{-1}) over a wide range of the electromagnetic spectrum, from the X-ray and UV band till the infrared and radio bands. AGNs are compact regions in the centre of galaxies, referred to as active galaxies. The central engines that power AGNs are accreting supermassive black holes with a black hole mass between $10^6 - 10^9$ M$_\odot$.

The term active galactic nuclei represents a very broad and diverse group of extragalactic sources, which have considerably different properties and emission features. Therefore the classification and unification of AGNs is an important step in order to reveal and understand the main physical processes involved in the triggering and fuelling of these sources. The study of AGNs is also important in terms of galaxy evolution, as AGNs can have a significant impact on their surroundings through feedback processes.

3.1 Classification of AGN

General references: Urry & Padovani (1995), Tadhunter (2008)
The classification of AGNs is a complex method based on several critiria, e.g. energetics, optical and UV spectral features, optical and radio morphology, spectral shape, luminosity and variability. The most commonly used classification method divides AGNs into three main groups basen on their optical and UV spectra, called Type 1, Type 2 and Type 0. These groups can be divided into several subgroups based on radio luminosity and nuclear luminosity. Another way to classify AGNs is to look at their energetics and the main form of their energy output.

Classification based on optical and ultraviolet spectra

Type 1 AGN
The spectra of Type 1 AGNs have bright continua and contain broad (typically $1000 - 2000$ km s^{-1}) permitted and semi-forbidden emission lines from hot, high velocity gas. In addition to the broad emission lines, most Type 1 AGNs show strong, high-ionization narrow emission lines. The group of radio-quiet Type 1 AGN contains Seyfert 1 galaxies and radio-quiet quasi-stellar objects (QSO). Seyfert 1 galaxies are relatively low luminosity, lower redshift spiral galaxies, their host galaxies can be often resolved. On the contrary, QSOs are much more luminous, which makes the observation of their host galaxies impossible in the optical regime. The radio-loud subgroup of Type 1 AGNs consists of the low luminosity broad line radio galaxies (BLRG) and high luminosity radio-loud quasars (RLQ), which can be further divided depending on the shape of their radio spectra: steep radio spectrum dominated or flat radio spectra dominated RLQs.

Type 2 AGN
Type 2 AGNs show only strong narrow emission lines and apparently no broad emission lines. Such sources are Seyfert 2 galaxies and narrow line X-ray galaxies in the radio-quiet subgroup and narrow line radio galaxies in the radio-loud subgroup. Some of these AGNs are actually Type 1 sources but the broad emission lines are hidden and can be only seen in polarized light. On the other hand, there are sources refered to as "real" Type 2 AGNs, which do not have any detectable broad lines. These AGNs have lower luminosities compared to Type 2 sources with hidden broad emission lines.

Type 0 AGN
A small fraction of radio-loud AGNs are collectively called blazars. These AGNs are highly variable sources, with their relativistic jets oriented close to the line-of-sight. Some of these AGNs have no strong emission and absorption features in their spectra, such as BL Lacertae (BL Lac) objects. Optically violently variable (OVV) quasars have similar continua to BL Lac objects but their optical/UV spectra has a feature called "Big Blue Bump" inspite of their strong synchrotron radiation.

Radiative-mode and jet-mode AGN

General references: Heckman & Best (2014)
Heckman & Best (2014) presented strong empirical evidence that the local AGN population can be divided into two major groups based on their energetics, by deriving their Eddington ratio, which is the ratio of AGN bolometric luminosity and the Eddington luminosity. The Eddington luminosity sets an upper limit to

the luminosity of a spherically accreting object with a given mass (M):

$$L_{Edd} = \frac{4\pi G m_{\rm p} c}{\sigma_T} M_{\rm BH} = 1.5 \times 10^{38} \frac{M_{\rm BH}}{M_\odot} \,{\rm erg\,s^{-1}} \tag{3.1}$$

where $m_{\rm p}$ is the mass of a proton, c is the speed of light and $\sigma_{\rm T}$ is the Thompson cross-section for electron scattering (Netzer 2015). Above this luminosity the object is not in equilibrium anymore, the radiation pressure exceeds the gravitational force and the gas will be blown away by the radiation. AGNs with high Eddington ratio ($\rm L_{bol}/L_{Edd} \gtrsim 0.01$) are called radiative mode AGN or high-ionization AGN. Their main energy output is in the form of electromagnetic radiation, which is produced by effective gas accretion through an optically thick accretion disk. Approximately 10% of these source are radio-loud. AGNs with lower Eddington ratio ($\rm L_{bol}/L_{Edd} \lesssim 0.01$) are jet-mode or low-ionization AGN and the main energy output is through kinetic energy transported by jets, powered by radiatively inafficient accretion flows (RIAF) or advection dominated accretion flows (ADAF).

Both radiative mode and jet-mode AGNs are found over the full range of radio powers but a characteristic switch happens around $P_{4.1\,\rm GHz} \sim 10^{25}\,\rm W\,Hz^{-1}$. Above this radio power, radio sources are mostly radiative mode AGN, below this value the majority of radio-loud AGNs are jet-mode. At higher redshift ($z > 1$) radiative mode AGNs dominate at all radio luminosities, while in the local Universe jet-mode AGNs dominate the radio population except the highest radio luminosity sources. Regarding their host galaxies, radiative mode radio-loud AGNs are associated with on-going star formation in their hosts, while the host galaxies of jet-mode AGNs are red and passive.

Radiative and jet mode AGNs can be further divided into subgroups based on their emission spectra and radio-power:

- Radiative mode Type 1 AGNs have both broad permitted and narrow emission lines in their spectra and can be radio-loud quasars or radio-quiet QSOs and Seyfert 1 galaxies.
- Radiative mode Type 2 AGNs have only strong narrow emission lines in their spectra and can be high-excitation radio sources or radio-quiet QSOs and Seyfert 2 galaxies.
- Jet-mode AGNs have weak to moderate strength narrow, low-ionization emission lines and can be low-excitation radio sources or LINERS (galaxies with low-ionization nuclear emission line regions).

Fanaroff-Riley classification

Radio-loud AGNs can be classified on the basis of their extended radio structures (Fanaroff & Riley 1974). Fanaroff-Riley I (FR I) radio galaxies have bright inner

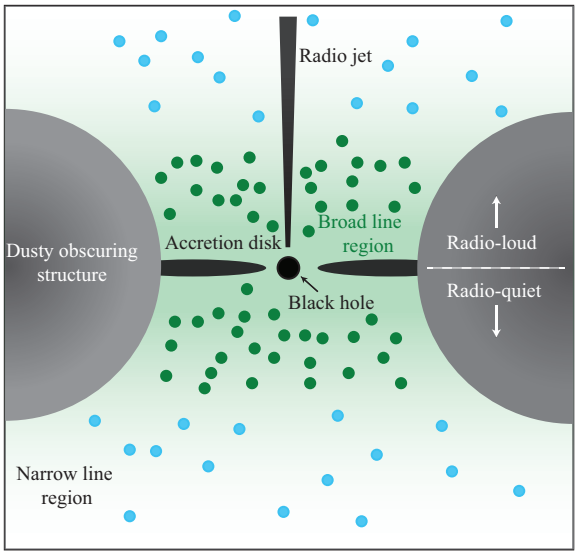

Figure 3.1: The schematic view of the central region of radiative-mode AGN based on Heckman & Best (2014).

jets but they flare and their intensity gradually decreases from the nucleus, while FR II radio galaxies have highly collimated jets, ending in prominent radio lobes and hot spots. FR II radio sources are generally more powerful, hence they are more efficient in transporting energy toward their lobes. In case of FRII radio sources the relativistic jets can maintain their energy as they propagate through the host galaxy, while the jets of FR I sources dissipate their energy due to the interaction with the surrounding medium.

The switch between FR I and FR II morphology is around $P_{4.1\,\mathrm{GHz}} \sim 10^{25}\,\mathrm{W\,Hz^{-1}}$. While there is an overlap between radiative mode AGNs and radio sources with FR II morphology, as well as between jet-mode AGNs and FR I radio sources, this is due to the similar radio power at which the switch occurs between these AGNs populations and does not mean that the radio morphology and the nature of the accretion flow depend on each other. Both radiative-mode FR I and jet-mode FR II radio sources exist.

3.2 The Unified Model of AGNs

General references: Antonucci (1993); Urry & Padovani (1995); Tadhunter (2008)
The Unified Model of AGNs proposes the idea that the only difference between Type 1/Type 2 AGN or radio-loud/radio-quiet AGNs is in their orientation relative to the observer's line-of-sight. The unification of AGNs has two important pillars, the effect of relativistic beaming and anisotropic obscuration by an optically thick region surrounded the AGN. Relativistic beaming means that the

apparent luminosity of the AGN seems higher if the radio jet is pointing closer to line-of-sight.

Figure 3.1 illustrates the schematic structure of the central part of AGNs. In case of radiative mode AGNs, the SMBH is fed by gas inflow from a geometrically thin, optically thick accretion disk. The accretion disk is surrounded by a hot corona, where photons are Compton-scattered up to X-ray energy levels. Both the accretion disk and the hot corona emit highly ionizing radiation, which photoionizes any dense clouds close to the nucleus. This region of high velocity gas ($\sim 1000\,\mathrm{km\,s^{-1}}$) associated with UV-to-near-IR permitted emission lines is called the Broad Line Region.

On larger scale, the accretion disk and the SMBH are surrounded by an obscuring, clumpy structure (often referred to as torus), which consists of dust and molecular gas ($N \sim 10^{23} - 10^{25}\,\mathrm{cm^{-2}}$). This obscuring structure is responsible for the thermal IR emission of AGN. In some cases the opacity of the torus is so high, that even the hardest X-ray photons cannot escape from it (Compton-thick). The only exit for the ionizing radiation coming from the accretion disk and corona is along the polar axis of the torus. These escaping photons photoionize gas clouds at higher distances from the SMBH. This region of lower density and lower velocity gas at a scale of $0.1 - 1\,\mathrm{kpc}$ is called the Narrow Line Region, from where the UV-to-IR forbidden and permitted narrow ($\sim 100\,\mathrm{km\,s^{-1}}$) emission lines originate.

Based on the above picture the unification scheme easily emerges. If the observer's line-of-sight is close to the polar axis of the torus, the AGN can be seen directly: in case of Type 1 AGN the SMBH, the accretion disk and the Broad Line Region is not obscured, therefore their observed spectra contain both narrow and broad emission lines. If the viewing angle of the AGN is closer to the equatorial axis of the obscuring torus, the AGN is obscured. The spectra of these obscured, Type 2 AGNs only contain narrow emission lines, since the Broad Line Region is hidden.

In case of radio-loud AGNs the combination of the orientation effects and the relativistic beaming is necessary to explain the observed differences between radio-loud quasars and radio galaxies, such as the lack of broad permitted lines and Big Blue Bump continuum emission in radio galaxies (Barthel 1989). When the radio jet is oriented in a large angle relative to the line-of-sight, the central part of the AGN is hidden by the dusty circumnuclear torus and the object can be observed as a narrow line radio galaxies. If the radio jet is pointing closer to the line-of-sight, the central AGN becomes visible and the AGN is classified as a quasar, with steep radio spectrum. At a very small angle between the radio jet and the line-of-sight, the relativistic jets are beamed and the AGN is dominated by the flat radio spectrum and is observed as a higly variable, blasar or an OVV quasar.

3.3 The role of AGN-feedback

General references: Fabian (2012); Heckman & Best (2014)
AGN feedback is the interaction of the central SMBH and its host galaxy through the energy and radiation generated by the accreting SMBH. As the binding energy of an accreting SMBH is significantly larger than that of the bulge, the feedback from the AGN must have a great impact on its host galaxy. AGN feedback has two distinct modes based on the nature of the energy outflows near the SMBH, radiative mode (quasar or wind mode) and kinetic mode (radio-jet or maintenance mode).

The radiative mode AGN feedback requires radiatively efficient accretion flow, thus it occurs in sources with high Eddington ratio: in case of luminous quasars and AGNs and generally in the early, young stages of these sources. This feedback mode was probably most effective at the peak of quasar activity ($z \sim 2-3$), when galaxies were more gas-rich. Radiative mode feedback can act in form of radiation pressure on the surrounding medium, specifically on dust grains or in form of AGN winds and outflows.

In case of radiation pressure driven feedback, the UV emission radiated by the AGN is easily absorbed by dust grains, which reradiate them in the IR regime. If the surrounding gas is optically thick, these IR photons can undergo multiple scattering while momentum flux is transferred to them. As a result radiation pressure can drive a shell of dusty gas into the host galaxy. However, this radiation-powered flow can only move outward until the medium is optically thick.

Interaction may occur through high velocity winds, observed as line absorption in the AGN continuum or galactic scale outflows, with outflow rates of hundreds to thousands $\mathrm{M}_\odot\,\mathrm{yr}^{-1}$ and velocities up to thounsands of $\mathrm{km\,s}^{-1}$ (e.g. Walter et al. 2002; Prochaska & Hennawi 2009; Morganti et al. 2007; Feruglio et al. 2010; Nesvadba et al. 2011; Aalto et al. 2012; Greene et al. 2012; Rupke & Veilleux 2013). Given the high velocities and outflow rates, radiative mode AGN feedback is the only plausible explanation to their origin. Such outflows are able to expel the gas from the host galaxy and quench star formation, thus regulating the growth of both the SMBH and the host galaxy: the galaxy is moving from the blue, star-forming sequence to the red sequence of galaxies. Thus radiative mode feedback may be responsible for setting up the observed correlations between black hole mass and bulge properties.

Kinetic mode feedback operates in lower redshift, massive, "red and dead" galaxies, typically living in the centers of galaxy groups and clusters. However, they are surrounded by X-ray emitting gas with cooling times in the central regions of the clusters shorter than the Hubble time, which would result in cooling flows with cooling rates of thousands of $\mathrm{M}_\odot\,\mathrm{yr}^{-1}$ in the absence of feedback mechanisms. This huge amount of gas would boost the star formation and the stellar mass of the galaxy would significantly grow. But something acts against the cooling: main-

tenance mode AGN feedback. According to the general consensus, as the cooling of the gas begins in the central regions and reaches the SMBH it will generate powerful jets, which inject energy back to the halo and the intracluster medium (ICM) by inflating bubbles of relativistic plasma in order to balance the energy loss by radiative cooling. Such bubbles or cavities are clearly seen in X-ray and radio observations (e.g. Boehringer et al. 1993; McNamara et al. 2000; Dunn & Fabian 2006, 2008). Hence this feedback maintains the "red and dead" state of the galaxy and the correlation between the SMBH and the bulge of its host galaxy.

3.4 The environment of high-z AGN

In order to gain insight into the formation and evolution of local massive elliptical galaxies one has to look back in time to find and study their progenitors. Since present-day galaxy clusters host hundreds of galaxies, which show a clear red sequence and merger events likely played an important role in building these massive galaxies, protoclusters might be the scene of these events (Dressler 1980; Vikhlinin et al. 2014; Overzier 2016). Protoclusters are overdense structures of galaxies at high redshift ($z > 2$), which are still forming and are not bound and virialised systems. Protoclusters are very extended, spread out till several tens of cMpc across (Chiang et al. 2013; Muldrew et al. 2015). The protocluster members, the progenitors of local massive ellipticals, are gas-rich and star-forming galaxies. As the most luminous high-z AGNs are massive galaxies themselves (Seymour et al. 2007), they likely live in overdense environment and can be used as tracers of protoclusters and dense regions. Indeed, studies of high-z powerful AGNs found such overdensities of star-forming galaxies in their environment both at large and small scales using observational probes such as Lyα and Hα emission lines, mid-IR emission from stars or dust emission in submm and mm bands (e.g. Yates et al. 1989; Hill & Lilly 1991; Le Fevre et al. 1996; Best et al. 1998; Best 2000; Best et al. 2003; Donoso et al. 2010; Galametz et al. 2010; Hatch et al. 2011; Falder et al. 2011; Galametz et al. 2012, 2013; Cooke et al. 2014; Rigby et al. 2014; Adams et al. 2015; Husband et al. 2016; Ghaffari et al. 2017; Magliocchetti et al. 2018).

For instance, narrow band imaging of the high-z radio galaxy (HzRG) MRC 1138–262 ($z = 2.16$) found ~ 50 LAEs in its $8.3\,\mathrm{Mpc}^2$ field and subsequent spectroscopic observations confirmed that 15 of these sources are at the same redshift as the HzRG (Kurk et al. 2000, 2004b; Pentericci et al. 2000; Croft et al. 2005). Hα emission line studies of the field of MRC 1138–262 also showed overdensities of star-forming galaxies towards the radio galaxy (Kurk et al. 2004b,a). Moreover, Venemans et al. (2007) studied the $9\,\mathrm{Mpc}^2$ field of eight radio galaxies ($z = 2.1 - 4.1$) and searched for LAEs in their fields. In case of six fields they found a factor of $3 - 5$ overdensity of LAEs compared to the volume density of field Lyα emitters at similar redshifts.

Deep submm observations and MIR studies of luminous AGNs led to similar

conclusions. Stevens et al. (2003) used the Submillimetre Common-User Bolometer Array (SCUBA) on the James Clerk Maxwell Telescope (JCMT) to study seven HzRGs and found an overdensity of submm sources around their targets. A surprising feature of their findings is the observed alignments of the radio axis of HzRGs with their brightest submm sources, indicating that they trace the large-scale structure around the HzRGs. An excess of star-forming galaxies have been also discovered in case of X-ray and optically selected high-z quasars (Stevens et al. 2004; Priddey et al. 2008; Stevens et al. 2010).

The CARLA program (Clusters Around Radio-Loud AGN) used the Infrared Array Camera (IRAC) on board of *Spitzer Space Telescope* to investigate the environment of a large sample of radio loud quasars and HzRGs at $1.2 < z < 3.2$ (Wylezalek et al. 2013, 2014). During this program the field of 387 radio-loud AGNs have been observed in the $3.6\,\mu m$ and $4.5\,\mu m$ IRAC bands. To identify high-z sources in the field of the AGNs, the potential galaxy cluster members, they used the colour cut $[3.6] - [4.5] > -0.1\,(\mathrm{AB})$, which selects galaxies above $z > 1.3$. They found that $\sim$55% of the radio-loud AGN fields are overdense at 2σ level and $\sim$10% are overdense at 5σ level compared to sources selected similarly in blank fields. An interesting aspect of their results is that they did not find any sign of dependence of environment on radio luminosity and the fields of radio-loud quasars and HzRGs are quite similar.

In addition, submm observations of WISE (Wide-field Infrared Survey Explorer) and radio-selected, luminous AGNs discovered a factor of $4 - 6$ overdensity of submm galaxies in their 1.5 arcmin-radius environment compared to blank-field surveys, suggesting that WISE/radio selected AGNs are signposts of overdense regions of dusty, star-forming galaxies (Jones et al. 2015). Silva et al. (2015) found even higher excess of SMGs around WISE/radio selected hyper-luminous quasars ($z \sim 2$) using ALMA (Atacama Large Millimeter/submillimeter Array) at a scale of 150 kpc.

In summary, high-z AGNs can be used as tracers of galaxy overdensities on large scales. However, based on observations and semi-analytic models, HzRGs are hosted by the most massive haloes and are better signposts of protoclusters, compared to quasars (Donoso et al. 2010; Fanidakis et al. 2011a, 2013; Orsi et al. 2016; Mazzucchelli et al. 2017; Izquierdo-Villalba et al. 2018; Uchiyama et al. 2018; Champagne et al. 2018). In addition, radio-loud quasars at $z < 2.5$ are more strongly clustered compared to radio-quiet quasars with similar luminosity and SMBH mass (Shen et al. 2009). Hatch et al. (2014) found that the environment of radio-loud AGNs is significantly different from that of radio-quiet galaxies with similar masses. Based on their results the Mpc-scale environment of galaxies influences the probability of jet launching, thus the correlation between radio-loud AGN and high-density environment is not due to observational selection bias.

Looking at smaller scales, gas-rich, star-forming companion galaxies have been discovered for a number of high-z quasars and radio galaxies, in some cases these

systems are alreay in the early/late stage of a merger event (e.g. Ivison et al. 2000; De Breuck et al. 2005; Greve et al. 2007; Ivison et al. 2008; Riechers et al. 2008; Nesvadba et al. 2009; Clements et al. 2009; Ivison et al. 2012; Salomé et al. 2012; Riechers 2013; Husband et al. 2015; Gullberg et al. 2016; Trakhtenbrot et al. 2017; Banerji et al. 2017; Carniani et al. 2017; Decarli et al. 2017).

One of the many interesting sources is the quasar BR 1202-0725 ($z = 4.7$), which has a starburst companion at $\sim 25\,\mathrm{kpc}$ distance, while high-resolution ALMA observations discovered that both of these objects have even closer companion galaxies, indicating that this complex system is in a gas-rich, multiple merger event (Salomé et al. 2012). Another fascinating example is the quasar PKS 1614+051 ($z = 3.2$), which has four Lyα-emitting companion galaxies, from which three are in the close vicinity of the quasar, suggesting that they eventually merge into a massive galaxy by $z \sim 1$ (Husband et al. 2015).

While the host galaxies of high-z AGNs in the above systems are gas-rich and/or star-forming themselves, there are several AGN–companion galaxy systems, in which the host galaxy of the AGN seems gas-poor and/or most of the star formation is not happening in the AGN host but rather in companion galaxies (Clements et al. 2009; Nesvadba et al. 2009; Riechers 2013; Decarli et al. 2017). For instance, Clements et al. (2009) discovered extended submm emission offset from the quasar SDSS 160705+533558 ($z = 3.65$) and concluded that this object is an early stage of a merger event between the gas-poor host galaxy of the AGN and a gas-rich, starburst galaxy. The case of SMM J04135+10277 ($z = 2.8$) is very similar: while this quasar was discovered through its bright submm emission (Knudsen et al. 2003) and previous CO observations detected large amount of gas ($M_{\mathrm{H_2}} \sim 10^{11}\,\mathrm{M_\odot}$), recent CO(3-2) observations revealed that this massive gas reservoir is associated with an optically faint, gas-rich companion galaxy and not the quasar (Riechers 2013). If these systems undergo a merger event and build a massive elliptical by $z \sim 0$, then a significant fraction of the stellar mass of the forming elliptical galaxy was built up in the companion, while the SMBH of the forming elliptical grew in the host galaxy of the AGN. However, if this is the case, how is the well-known $M_{\mathrm{BH}} - M_{\mathrm{bulge}}$ correlation established? It might be that the SMBH also grows significantly during the merger through gas accretion supplied by the companion galaxy or through merger averaging, if the companion galaxy also harbours a SMBH.

The observed richness of star-forming, gas-rich galaxies in the large- and small-scale environment of HzRGs and quasars demonstrate the relevance of such studies in finding the progenitors of massive local galaxies, and the discovery of close high-z AGN–star-forming companion galaxy pairs and early/late mergers highlights the importance of high resolution observations in order to understand their formation.

Chapter 4

Introduction to radio astronomy

The Earth atmosphere is opaque across a large part of the electromagnetic spectrum and this in turn affects how we can observe space. High frequency radiation (γ-rays, X-rays, UV photons) and a large part of the infrared range is absorbed by the Earth's atmosphere, thus ground based astronomic observations are limited to optical, near-infared and radio wavelengths. The so-called radio window is between 15 MHz–1.5 THz. The high-frequency cut-off of the radio window is due to resonant absorption of atmospheric molecules, mainly H_2O and O_2. At low frequencies the ionosphere of the Earth reflects back radiation with frequencies below the plasma frequency. These boundaries are not sharp, the former depends on altitude and geographical position, the latter varies with space weather and daytime/night-time.

Since the radio window is very broad, many different emission features can be observed (e.g. thermal dust emission, molecular and atomic spectral lines, synchrotron emission), which probe a large range of physical mechanisms and astronomical phenomena (e.g. stellar physics, search for planetary systems in formation, ISM, galaxies, Sunyaev–Zel'dovich effect, masers). Depending on the target source different radio telescopes and antenna arrays can be used. An important factor of radio observations is the angular resolution $\Theta \sim \lambda/D$, which depends on the observing wavelength λ and the diameter D of the antenna. Because of the long wavelength of radio waves, the resolution is limited when using small antennas. Single-dish telescopes are relevant for observations of the local Universe, or to trace extended, low surface brightness emission in more distant sources or serve as source finding tools for follow-up observations with better capabilities. However, to detect faint or high-redshift sources we need interferometric observations. In this chapter I summarise the basics of single-dish and interferometric observations and give an overview of the observing facilities, which supplied the data presented in the appended papers.

4.1 Single-dish basics

General references: Wilson et al. (2009); Condon & Ransom (2016)
A radio telescope consists of two main components: the antenna, which collects the incoming radio waves, and a receiver and amplifier component, which boosts the incoming weak signal. Let's consider a parabolic dish antenna. How well the antenna can receive the incoming radiation depends on the position of the source relative to the antenna. The so called normalized power pattern or radiation pattern of the antenna describes the direction and shape of the beam.

$$P_{\rm n}(\theta,\phi) = \frac{1}{P_{\rm max}} P(\theta,\phi), \tag{4.1}$$

where $P_{\rm max}$ is constant and $P(\theta,\phi)$ is the total power pattern including the main beam (MB) and side lobes (SL). The beam solid angle is defined as

$$\Omega_{\rm A} = \int\int P_{\rm n}(\theta,\phi) d\Omega = \Omega_{\rm MB} + \Omega_{\rm SL}. \tag{4.2}$$

The beam size of the antenna is the full width at half maximum (FWHM) of the main beam and defines the angular resolution, which is diffraction-limited: $\Theta_{MB} \sim \lambda/D$.

Another important characteristic of the antenna is its affective aperture $A_{\rm e}$, the ratio of the power density P_ν detected by the antenna and the incoming flux S_ν.

$$A_{\rm e} = \frac{2P_\nu}{S_\nu} = \frac{\lambda^2}{\Omega_{\rm A}} \tag{4.3}$$

The power output per unit frequency from a receiving antenna can be expressed in terms of the antenna temperature $T_{\rm A}$. The antenna temperature is not the physical temperature of the antenna but that of a matched resistor, whose thermally generated power per unit frequency equals the power produced by the antenna. $T_{\rm A}$ is the sum of several components contributing to the external noise of the system, including the source, the sky, the ground, the cosmic microwave background etc. $T_{\rm A}$ can be expressed using the Nyquist theorem and the effective aperture:

$$T_{\rm A} = \frac{P_\nu}{k} = \frac{A_{\rm e} S_\nu}{2k}. \tag{4.4}$$

In order to connect the antenna temperature, which we can measure, to the brightness temperature of the source $T_{\rm b}$, we can express $T_{\rm A}$ as the convolution of the brightness temperature with the beam pattern of the telescope:

$$T_{\rm A} = \frac{\int\int T_{\rm b}(\theta,\phi) P_{\rm n}(\theta,\phi) d\Omega}{\Omega_{\rm A}}. \tag{4.5}$$

If the source is extended and has a constant brightness temperature, then

$$T_{\rm A} \approx \frac{\Omega_{\rm MB}}{\Omega_{\rm A}} T_{\rm b}. \tag{4.6}$$

If the source size is much smaller compared to the beam ($\Omega_{\rm S} \ll \Omega_{\rm A}$) and both the brightness distribution of the source and the beam have Gaussian shape, then

$$T_{\rm A} \approx \frac{\Theta_{\rm S}^2}{\Theta_{\rm S}^2 + \Theta_{\rm MB}^2} T_{\rm b}. \tag{4.7}$$

The total noise of the system is system noise temperature $T_{\rm sys}$, which includes $T_{\rm A}$ and noise from the receiver $T_{\rm R}$.

$$T_{\rm sys} = T_{\rm A} + T_{\rm R} \tag{4.8}$$

The rms noise per channel is given by the radiometer equation of a total power receiver:

$$\Delta T = \frac{T_{\rm sys}}{(\Delta\nu\tau)^{1/2}} \tag{4.9}$$

where $\Delta\nu$ is the bandwidth of the observation and τ is the total integration time. The point source sensitivity can be derived from the radiometer equation and for a single antenna is

$$\sigma_{\rm S} = \frac{2kT_{\rm sys}}{A_{\rm e}(\Delta\nu\tau)^{1/2}} \tag{4.10}$$

Atacama Pathfinder Experinment

The Atacama Pathfinder Experinment (APEX) telescope is located in Llano de Chajnantor, in northern Chile, in the Atacama desert. APEX is a modified ALMA prototype telescope, with a dish size of 12 m and beam width of $\sim 7.8'' \times (800/\nu\,[\mathrm{GHz}])$. APEX is a collaboration between the Max Planck Institute for Radio Astronomy, the Onsala Space Observatory and the European Southern Observatory. APEX is also part of the Event Horizon Telescope and the global mm-VLBI network. Several instruments can be mounted on APEX, such as the bolometer araray LABOCA operating at 870 μm (345 GHz) or SEPIA, a Swedish PI receiver for APEX operating in band 5 (159-211 GHz) and band 9 (578-738 GHz).

In Paper I we present new APEX ArTeMiS data at 350 μm of the quasar SMM J04135+10277. ArTeMiS is a large bolometer camera operating in the submm range.

4.2 Radio interferometry basics

General references: Taylor et al. (1999); Wilson et al. (2009); Condon & Ransom (2016)

The essence of radio interferometry lies in the possibility to connect multiple antennas, either on-site as antenna arrays or across the Earth as part of global interferometric arrays, to act as one huge antenna, which significantly increases the sensitivity and resolution of the observation. Instead of the dish diameter of the individual antennas, the resolution is determined by the longest separation between antenna pairs, referred to as the longest baseline. The sensitivity of an interferometer depends on the effective aperture or effective area A_e of the interferometric array and increases with the number of antennas used during the observation. An interferometer consisting of N dishes has a point source sensitivity of

$$\sigma_\mathrm{S} = \frac{2kT_\mathrm{sys}}{A_\mathrm{e}(N(N-1)\Delta\nu\tau)^{1/2}} \tag{4.11}$$

where T_Sys is the system noise tempreature, $\Delta\nu$ is the bandwidth of the observation and τ is the total integration time.

The simplest interferometer is a two-element array, where the output voltage of the antennas are correlated (multiplied and averaged). The baseline vector $\vec{b}$ points from antenna 1 to antenna 2 and both antennas observe the same source with a unit vector $\vec{s}$ pointing towards it and at θ angle from the baseline vector (Fig. 4.1). While the output voltage of both antennas is the same, there is a time delay between the two antennas receiving the signal from the source, called as the geometric delay:

$$\tau_\mathrm{g} = \frac{\vec{b}\vec{s}}{c} \tag{4.12}$$

To demonstrate how radio interferometry works let's consider a stationary, two element, quasi-monochromatic interferometer, with a very narrow bandwidth of $\Delta\nu \ll 2\pi\tau_\mathrm{g}$ and centred on frequency $\nu = \omega/(2\pi)$. The electric field produced by the source can be expressed in term of voltages: $V_1 = V\cos[\omega(t-\tau_\mathrm{g})]$ and $V_2 = V\cos(\omega t)$. The correlator then multiplies these voltages and takes their time average:

$$\langle V_1 V_2\rangle = \left(\frac{V^2}{2}\right)\cos(\omega\tau_g). \tag{4.13}$$

The amplitude of the correlator output is proportional to the flux density of the source multiplied by the root-square of the effective collecting areas of the antennas, $(A_1A_2)^{1/2}$. When the interferometer observes a spatially incoherent, slightly extended source with a brightness $I_\nu(\vec{s})$, its correlator response is

$$R_C = \int I_\nu(\vec{s})\cos(2\pi\nu\vec{b}\vec{s}/c)d\Omega. \tag{4.14}$$

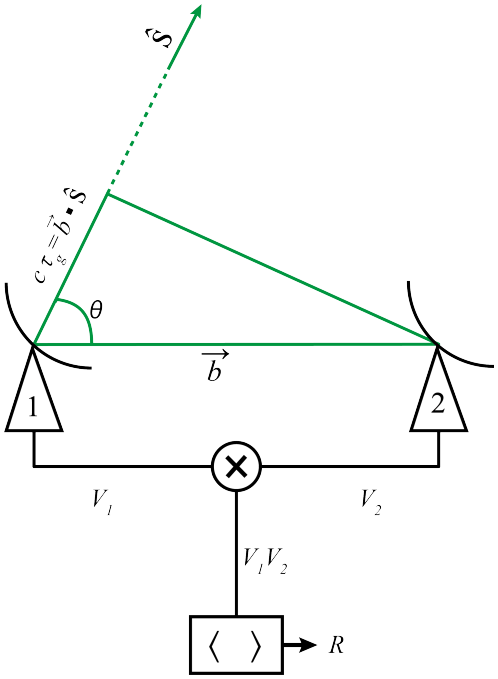

Figure 4.1: Two-element radio interferometer.

Thus the interferometer response, which we can measure is linked to the source brightness, which can be expressed as a sum of an even and an odd part, $I = I_{\mathrm{E}} + I_{\mathrm{O}}$. However, the cosine fringe pattern is even, thus it is not sensitive to the odd part. To solve this another correlator response is necessary:

$$R_S = \int I_\nu(\vec{s}) \sin(2\pi\nu\vec{b}\vec{s}/c) d\Omega. \tag{4.15}$$

Based on these the complex visibility can be defined as

$$V = R_C - iR_S = \int I_\nu(\vec{s}) e^{(-i2\pi\nu\vec{b}\vec{s}/c)} d\Omega = Ae^{i\Phi}, \tag{4.16}$$

where the visibility amplitude and phase is

$$A = (R_C^2 + R_S^2)^{1/2} \text{ and } \Phi = \tan^{-1}\frac{R_S}{R_C}. \tag{4.17}$$

By introducing the (u, v, w) coordinate system, where the components of the baseline vector $\vec{b}/\lambda$ are in wavelength units with u and v pointing towards east and north defining the $u - v$ plane where the antennas lie $(w = 0)$, and w as the axis normal to the $u - v$ plane, the visibility can be expressed as

$$V_\nu(u, v) = \int\int I_\nu(l, m) e^{-i2\pi(ul+vm)} dl dm. \tag{4.18}$$

According to the van Cittert-Zernike theorem the complex visibility is the Fourier transform of the source brightness distribution measured at the points of the $u-v$ plane given by the baselines. In order to get the brightness of the source, the visibility needs to be inverted:

$$I_\nu(l,m) = \int\int V_\nu(u,v) e^{i2\pi(ul+vm)} du dv. \tag{4.19}$$

The interferometer at any given time measures the visibility at the baseline coordinates u, v. However, the sampling of the $u-v$ plane is not complete, the interferometer only observes a small fraction of it. However, as the Earth rotates the telescope positions change relative to the source position and this Earth-rotation aperture synthesis can be utilised to synthesis better $u-v$ coverage.

While the point-source sensitivity of an interferometer and a single-dish antenna with the same total effective area is comparable, the interferometer has a much worse sensitivity to low surface brightness sources, as its synthesized beam solid angle is much smaller than the beam solid angle of a single dish with the same total effective area. Another limitation of interferometers arises from the incomplete $u-v$ coverage at spacings smaller than the minimum baseline. Thus for the interferometer extended emission with angular size smaller or comparable to $\lambda/b_{\rm min}$ is invisible, the emission is resolved out. To detect such large-scale emission the use of single-dish telescopes is necessary.

Atacama Large Millimeter/submillimeter Array

The Atacama Large Millimeter/submillimeter Array (ALMA) is the most powerful and sensitive telescope in the mm/submm wavelength regime and the largest international collaboration for mm astronomy, involving partners from Europe, North America, and East Asia. ALMA is located in the Chajnantor plateau in northern Chile, at 5000 m altitude. It consist of 66 antennas gathered in two different arrays: the 12-m array and the compact array (ACA), which has 12 7-m antennas and 4 12-m antennas. ALMA has observing bands starting from band 3 (84 GHz) till band 10 (950 GHz). The resolution in the most compact configuration is between $0.5'' - 4.8''$, while in the most extended configuration it reaches $0.02'' - 0.04''$.

Paper II and III present new continuum and line emission data observed by ALMA in band 3, 4 and 6, tracing dust emission and CO(3–2), CO(5–4) and CO(8–7) line emission from two AGNs, SMM J04135+10277 and TXS 0828+193.

Karl G. Jansky Very Large Array

The Karl G. Jansky Very Large Array (JVLA) is located at the Plains of San Agustin, New Mexico, USA, run by the National Radio Astronomical Observatory. It consists of 27+1 antennas, each with a diameter of 25 m. The array has a

characteristic Y-shape. It operates in four different configurations (A, B, C, D), A being the most extended, D being the most compact. The achieved resolution of JVLA is around $0.2'' - 0.04''$. Its different observing bands are sensitive to emission from 1 GHz to 50 GHz.

Paper IV presents continuum and CO(1–0) line emission data of a high-z quasar SDSS 160705+533558, observed in K band and D configuration.

Chapter 5

Introduction to the appended papers

5.1 Modelling of the spectral energy distribution

General references: Conroy (2013)
The spectral energy distribution (SED) shows the energy output of a galaxy over the electromagnetic spectrum (Figure 5.1). As galaxies have many different building blocks (old and young stars, gas, dust, AGN etc.), each of these components influence the final shape of the SED. Old, lower mass stars are cooler, thus they emit their energy in the red end of the optical band and in the NIR, while hot, young, massive stars are bright in the blue part of the optical band and in the UV. Dust is an important tracer of star formation and hidden AGN, as it absorbs the UV and optical light and reemits it in the infrared. If the galaxy harbours an AGN, it can have a significant contribution to the final galaxy SED in the X-ray, UV, optical, IR and radio bands. Two important SED features that indicate the presence of an AGN are the "Big Blue Bump", which is related to thermal emission from the accretion disk and the IR bump, which originates from thermal emission from dust at a wide range of temperatures. Since the SED of galaxies contain fundamental information about their stellar populations, star-formation history, gas and dust content and their overall evolution, disentangling the observed SEDs is of great importance. SED modelling is a powerful tool to extract information from the observed SEDs. Stellar population synthesis (SPS) models are widely used and have become very popular.

The first ingredient of SPS models is a simple stellar population (SSP), which represents the time evolution of a single population of coeval stars with a given metallicity and abundance pattern. To construct the SSP one has to combine stellar evolution theory in form of isochrones, stellar spectral libraries and the initial mass function (IMF). An isochrone specifies the location of stars with the same age and metallicity on the Hertzsprung-Russel diagram and are constructed from stellar evolution calculations. Stellar spectral libraries contain a large set

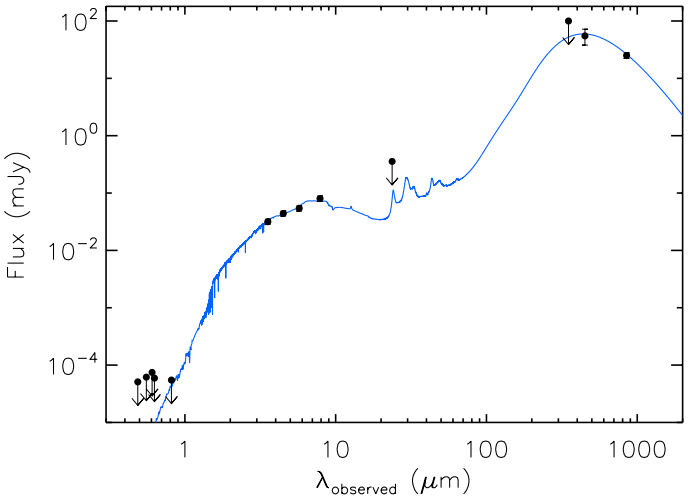

Figure 5.1: The spectral energy distribution of the companion galaxy of SMM J04135+10277, included in **Paper I**. The blue curve indicates the dust attenuated MAGPHYS model of the SED.

of stellar spectra with different metallicity, effective temperature and luminosity and can be constrained from empirical studies or purely theoretical models. The IMF describes the initial stellar mass distribution of a stellar population entering the main sequence on the Hertzsprung-Russel diagram. The initial mass is a very important parameter of stars, since it determines their lifetime, luminosity and the chemical enrichment of the ISM. The most popular IMF models are the Salpeter, Kroupa, and Chabrier (Salpeter 1955; Kroupa 2002; Chabrier 2003) models. The next step of SPS models is to construct composite stellar populations by combing simple stellar populations with different ages and metallicities with the effect of dust (attenuation and emission). The effect of nebular emission on the SED also needs to be taken account as its contribution to the broadband fluxes can be high, thus it can have a significant impact on the derived parameters.

By modelling the SED, several important parameters can be derived, such as the stellar mass, star formation rate, star-formation history, metallicity, dust attenuation. Moreover, in case of high-z studies, the SED can be used to determine photometric redshifts, if spectroscopic redshifts are not available. The infrared emission of dust grains provides additional information about the physical properties of a galaxy, including dust luminosity, dust temperature and dust mass. The dust temperature of star-forming galaxies is typically $\sim 30-60\,\mathrm{K}$, while AGN have higher dust temperature ($T_{\mathrm{dust}} \gtrsim 60-100\,\mathrm{K}$).

In Paper I we present SED modelling using the MAGPHYS code with high-z extensions (da Cunha et al. 2008, 2015). MAGPHYS is one of the commonly used

SED fitting codes (e.g. Lanz et al. 2013; Rowlands et al. 2014; Smolčić et al. 2015). MAGPHYS models the star formation history, dust attenuation and metallicity of galaxies and combines the stellar emission with dust emission using energy balance technique. To compare the model SED with the observed, a Bayesian approach is used. The optical model library of the code is derived using the Bruzual & Charlot (2003) population synthesis code and the attenuation by dust is included via the two-component model of Charlot & Fall (2000). The infrared model library is computed by combining the infrared emission from stellar birth clouds and the ambient ISM. The main advantage of the MAGPHYS code is the consistent modelling of the ultraviolet-to-infared spectral energy distribution of galaxies. However, compared to other SED fitting tools, it is not possible to control or fix the fitting parameters.

In Paper II we present SED modelling using the multi-wavelength SED fitting procedure MR-MOOSE (Drouart & Falkendal 2018). MR-MOOSE is designed to fit the SED of single and blended sources in a Bayesian framework, treat upper limits consistently and use data sets with a range of observation sensitivities and spectral/spatial resolutions. Thus, MR-MOOSE enables the combination of low- and high-resolution data at the same photometric band. During the fitting several analytic models can be included to decribe the underlying physical processes, such as a blackbody model, an empirical AGN model, a single power-law model, a modified blackbody function. The code output files include convergence and triangle plots and the fitted SEDs, making the further analysis and interpretation of the fitted SED user-friendly.

One limitation of MR-MOOSE is the execution time, which depends on the complexity of a given configuration. Thus, an execution with many parameters and components can take several hours to finish. Another limitation lies in the initial values chosen for the fitting, which even more important when upper limits are included. If the initial values are far from the true values, the code will take a long time to converge. Finally, the implementation of more detailed models would improve the fitting procedure.

In Paper II in addition to MR-MOOSE we use an alternative approach for SED fitting, using the empirical SED model library of Chary & Elbaz (2001), which contains 105 SED templates with a wide range of infrared luminosities. The templates are based on SEDs of four prototypical galaxies (Arp 220, NGC 6090, M82 and M51), representing ultraluminous infrared galaxies, luminous infrared galaxies, startbursts and normal galaxies, generated by the Silva et al. (1998) models. The MIR part of the SEDs are replaced by ISOCAM CVF observations. The final templates were generated by interpolating between the model SEDs of the four galaxies and using additional FIR templates from Dale et al. (2001) to span a larger range of FIR spectral shapes.

5.2 Semi-analytical modelling of galaxy formation

While the evolution of dark matter haloes in the ΛCDM model is well understood, the evolution of the baryonic component is more complex, since it involves many processes, which also interact and influence each other (e.g. star formation, feedback from supernovae and AGN). New observational techniques and improved instrumentations allow us to look back further in time and study the cosmic evolution of galaxies. However, to understand the observations and thus the evolution of galaxies, we need to combine numerical simulations and semi-analytical models with the observations.

Semi-analytical models of galaxy formation and evolution can be used to interpret the observations and give predictions within the framework of the hierarchical evolution of dark matter haloes, without the resolution limitation of numerical simulations. These models use simple, analytical models to calculate the evolution of the baryonic component and generate merger trees to trace the hierarchical structure formation (e.g. Cole et al. 2000a; Baugh 2006). Semi-analytical models are flexible, many process can be modelled together and a wide range of galaxy properties can be calculated. The main limitations of semi-analytical models are the need for simplifying assumptions (e.g. spherical symmetry) and that some processes are modelled in a deterministic way (e.g. supernova feedback). However, as we learn more about the details of each process that plays an important role in the evolution of galaxies, the models can be improved and the paramateres can be updated.

In Paper I we present simulation results performed by a new development of the GALFORM semi-analytical cosmological model, developed mainly at Durham University, implemented in a new Millenium Simulation run with *WMAP7* cosmology (Cole et al. 2000b; Komatsu et al. 2011; Lagos et al. 2012; Gonzalez-Perez et al. 2014). GALFORM models all the important processes that determine the formation and evolution of galaxies: the collapse and merging of dark matter haloes; gas heating and cooling through shocks and radiative cooling inside dark matter haloes, leading to the formation of galactic disks; star formation; feedback from supernovae, AGN and from the photoionization of the IGM; chemical enrichment of gas and stars; galaxy mergers leading to the formation of stellar spheroids and collapse of gravitationally unstable disks. The galaxy luminosities are determined by combining the star formation and metal enrichment histories with SPS models for each galaxy. The attenuation of starlight by dust is included based on radiative transfer canculations. The model also includes a sophisticated model of black hole growth and AGN feedback. The final output of the simualtion is a prediction of the number and properties of galaxies that reside within the dark matter haloes of different masses. The detailed description of GALFORM can be found in Fanidakis et al. (2011b, 2012); Lagos et al. (2012); Gonzalez-Perez et al. (2014)

5.3 Spectral line energy distribution modelling

General references: Carilli & Walter (2013)
The CO spectral line energy distribution (CO SLED), often called as the CO excitation ladder, describes the relative rotational level populations. Through the modelling of the CO SLED we can constrain the average properties of the molecular gas, such as its temperature and density. In addition, CO SLED modelling can provide a better way to estimate the mass of the molecular gas in high-z galaxies, as the higher-J transitions are easier to observe than the CO(1-0) ground transition for such sources. Thus, to derive molecular gas masses one needs to convert the observed high-J line luminosity to the luminosity of the CO(1–0). Without modelling the SLED, this conversion can be made assuming thermalized level populations, comparing the SLED to that of galaxies selected by the same methods (e.g. SMGs) or to galaxies which have similar SFR and luminosity. However, galaxies selected by the same method or having similar physical properties can have very different SLEDs, thus very different excitation properties.

The best way to avoid these caveats is to model the SLED of a galaxy, provided there are sufficient number of observations both at low- and high-J levels. There are several techniques to do this, for instance using escape probability/large velocity gradient models, or photon-dominated region and/or X-ray dominated region models. While there are several assumptions and simplifications going into these models, they enable us to unfold the excitation conditions of individual high-z galaxies and to put a constraint on the general properties of different galaxy populations. For the majority of quasars their CO excitation can be modelled by a single temperature and density model, with temperatures of $40 - 60\,\mathrm{K}$ and gas density of $3.6 - 4.3\,\mathrm{cm}^{-3}$ (e.g. Riechers et al. 2006, 2009; Carilli & Walter 2013). However, the molecular gas in SMGs is less excited and they show an excess emission in the ground transition, thus their CO SLED modelling requires a two component model, consisting of a cold component responsible for the excess emission and a warm component at mid- to high-J leveles (e.g. Bothwell et al. 2013).

In Paper II we present CO SLED modelling using the non-LTE radiative transfer code RADEX, which uses escape probability formulation without large-scale velocity fields, assuming homogeneous and isothermal medium (van der Tak et al. 2007). RADEX solves the radiative transfer equation focusing on bound-bound transitions in a multi-level molecule, considering spontaneous downward rates, colllisional rates and stimulated transitions. While the main collisional partner is molecular hydrogen, up to seven collisional partners can be included in the calculations. RADEX assumes statistical equlibrium instead of LTE, as the latter does not hold for lower density gas of the ISM. To simplify the calculations RADEX infers the global properties of interstellar clouds and introduces the geometrically averaged escape probability of photons, which only depends on the optical depth. The background radiation field adopted by RADEX consists of several components, such

as the CMB radiation at a given redshift, the average Galactic starlight radiation at the UV to NIR part of spectrum and the model of the Galactic thermal dust emission at the FIR to mm part of the spectrum. The program starts from optically thin statistical equlibrium for the initial level populations and solves the problem iteratively. The output of the RADEX is the background subtracted line intensity.

The adventage of RADEX is its simplicity with limited amount of free parameters, while still provinding good first estimates of the average gas properties of the molecular gas. However, RADEX has some limitations compared to other models, such as the escape probability does not take into account contribution from the dust opacity and free-free opacity, the effects of line overlap are not considered, it cannot handle maser action, and does not include mechanical and X-ray heating, which might be important in the case of sources harbouring AGN.

Chapter 6

Summary of the appended papers

6.1 Summary of Paper I

In the appended paper we study the system of SMM J04135+10277 ($z = 2.84$), which consists of a SCUBA discovered type-1 quasar (Knudsen et al. 2003) and a gas-rich companion galaxy at $\sim 5''$ ($\sim 40\,\mathrm{kpc}$) distance from the AGN position. This system is particularly interesting, since the companion galaxy is associated with one of the most massive molecular gas reservoirs found in the high-z Universe ($M_{\mathrm{H_2}} \sim 10^{11}\,\mathrm{M_\odot}$), while the quasar seems to be gas-poor (Riechers 2013).

With the aim of investigating the properties of the companion galaxy of SMM J04135+10277, we use archive optical data (*HST* WFPC2, CFHT MegaPrime and MegaCam) and infrared (*Spitzer* IRAC and MIPS and SCUBA) and new APEX ArTeMiS 350 μm observations to construct its spectral energy distribution. The companion galaxy is not seen in the optical bands, only in the IRAC images, hence it was missed during the original identifications (Knudsen et al. 2003; Riechers 2013). To model the SED we use the SED fitting code MAGPHYS (da Cunha et al. 2008, 2015). Based on the SED modelling the companion galaxy of SMM J04135+10277 is a heavily dust obscured ($A_{\mathrm{V}} \gtrsim 2.8\,\mathrm{mag}$), star-forming galaxy with a star formation rate of $\sim 1000\,\mathrm{M_\odot\,yr^{-1}}$.

As in most quasar–star-forming galaxy systems the host galaxy of the quasar is also gas-rich, our main question is whether the case of SMM J04135+10277 is unique or common at high-z. In order to investigate the expected frequency of such systems, we use the cosmological semi-analytic model, GALFORM (Gonzalez-Perez et al. 2014). We take the outputs of the simulation at $z = 2.8$ to find quasar–companion pairs at different separations. We find that 22% of our simulated quasar sample have at least one companion galaxy in their $< 100\,\mathrm{kpc}$ environment and 0.3% have bright, star-forming companions ($\mathrm{SFR} > 100\,\mathrm{M_\odot\,yr^{-1}}$).

To make a direct comparison between the model predictions and the case of SMM J04135+10277, we focus on systems with an integrated SFR of $> 500\,\mathrm{M_\odot\,yr^{-1}}$

inside the aperture and compute their relative gas content and SFR. We find that in 67% of these systems the molecular gas masses of the quasars' host galaxies are lower compared to the integrated value of their companions at a distance of $< 50\,\mathrm{kpc}$ and the star formation is dominated by the companion galaxies and not the quasars' hosts. This means that the case of SMM J04135+10277 is representative of highly star-forming quasar–companion galaxy systems at $z = 2.8$. In the discussion section we compare our findings with observations of high-redshift quasars and HzRGs found in the literature.

My contribution to Paper I
I carried out the optical and near-infrared photometry of the companion galaxy and I was the PI of the APEX ArTeMiS observation. I carried out the data analysis, including the modelling of the spectral energy distribution of the companion galaxy. In addition, I was actively participating in the preparation of the simulation and in the interpretation of its results. I prepared the manuscript, except Section 4.1.

6.2 Summary of paper II

In this paper we continue to investigate the system of SMM J04135+10277 through ALMA CO(5–4) and CO(8–7) observations. Thanks to the high resolution of ALMA, both the quasar and its companion are detected in dust continuum for the first time, with the quasar having a $\sim 25\%$ contribution to the total dust emission. By fitting the FIR SED of the system using empirical templates and MR-MOOSE (Chary & Elbaz 2001; Drouart & Falkendal 2018), we estimate the star formation rate of the quasar and its companion to be $\sim 210 - 960\,\mathrm{M_\odot\,yr^{-1}}$ and $\sim 240 - 2400\,\mathrm{M_\odot\,yr^{-1}}$, respectively.

In contrast to previous CO $J = 3 - 2$ and $J = 1 - 0$ transition observations, we detect luminous CO(5–4) and CO(8–7) emission from both sources. The estimated molecular gas mass of the quasar host galaxy is $\sim (0.7 - 2.3) \times 10^{10}\,\mathrm{M_\odot}$, thus it cannot be considered gas-poor. The CO line profiles of the companion galaxy are very broad ($\sim 1000\,\mathrm{km\,s^{-1}}$) and show signs of rotation of a massive system. However, the angular resolution of the ALMA data is not sufficient to enable the proper analysis of the kinematics, and the observed line width is possibly affected by beam smearing.

The spectral line energy distribution (SLED) of the quasar and the companion was modelled using RADEX, a radiative transfer code (van der Tak et al. 2007). While due to the limited number of observations we cannot constrain well the excitation properties of the sources, RADEX could narrow down the possible density and temperature ranges.

The case of SMM J04135+10277 demonstrates the importance of having high-resolution, sensitive observations, including high-J CO transitions, in order to

establish a complete picture of a given system. Moreover, the detection of highly excited molecular gas in the host galaxy of the quasar indicates that one has to be cautious when interpreting non-detections of low-J CO lines in AGNs.

My contribution to Paper II
I was the PI of the ALMA observations; I imaged the data and carried out the data analysis including the modelling of the CO SLED of the sources, and I prepared the manuscript.

6.3 Summary of paper III

This paper focuses on the HzRG TXS 0828+193 ($z = 2.57$) and its large scale environment. TXS 0828+193 is a Fanaroff-Riley class II radio galaxy, with extended radio lobes ($\sim$ 100 kpc) and multiple hotspots (Roettgering et al. 1994; Carilli et al. 1997). Rest-frame UV observations show clumpy and asymmetric morphology (Pentericci et al. 1999). Based on *Spitzer* IRAC observations used in the Clusters Around Radio-Loud AGN (CARLA) program, the large scale environment of TXS0828+193 is overdense at $3 \geq \sigma$ level, implying that it resides in a rich galaxy cluster (Wylezalek et al. 2013).

An interesting feature of the HzRG is a luminous CO(3–2) line emitting region aligned with the axis of the radio jet, detected by the IRAM PdBI (Nesvadba et al. 2009), located $\sim 10''$ (80 kpc) south-west from the radio galaxy. The $5''$ beam size of the observation, corresponding to an upper size limit of ~ 40 kpc, does not allow to resolve the CO emitting region. The integrated CO spectrum shows two compact components, both having the same spatial position but different velocity offsets. The total molecular gas mass of the two components is $M_{H_2} \sim 1.4 \times 10^{10}\,M_\odot$. The CO emission region does not have a counterpart within the $5''$ beam in the shallow *Spitzer* IRAC and MIPS 24 μm images, nor in the optical.

With the aim of revealing the origin of the luminous CO emitting region, we observed the TXS 0828+193 with ALMA, obtaining high-resolution CO(3–2) and 100 GHz continuum measurements. As HzRGs are known for residing in overdense environment, we also search for additional companion galaxies in the field of the HzRG. In contrast to previous observations, we detect CO emission associated with the HzRG. The molecuar gas mass of the HzRG is $(0.9 \pm 0.3) \times 10^{10}\,M_\odot$. We confirm the presence of the previously detected off-source CO emitting region (companion #1), which is also detected in new, better quality IRAC images. This source might be a normal star-forming galaxy or alternatively a result of jet-induced star formation.

In addition, we detect three new potential companions, which show CO emission but have no counterparts in the 100 GHz continuum and in other observing bands. The molecular gas mass of each companion is comparable to that of the HzRG. These CO companions might be high-density clouds in the halo of the HzRG and

potentially linked to the large-scale filamentary structure of the cosmic web.

My contribution to Paper III
I led this project and paper through essentially all aspects: I did the source selection, was the PI of the ALMA observations, I imaged the data and carried out the data analysis and prepared the manuscript.

6.4 Summary of paper IV

In this paper we focus on the quasar SDSS 160705+533558 ($z = 3.653$). This is a broad absorption line quasar, which has strong MIR emission (Lonsdale et al. 2004; Hatziminaoglou et al. 2005; Trump et al. 2006). Based on its submm emission observed with SCUBA, it is one is one of the most luminous galaxies in the Universe, commonly referred to as Hyper Luminous Infrared Galaxies (HLIRG). However, follow-up high-resolution 850 μm observations using the Submillimeter Array (SMA) revealed that the peak of the submm emission is offset from the position of the quasar by 1.5″ (∼10 kpc; Clements et al. 2009). The observed submm offset and the presence of a submm tail towards south indicates that this source is a merger between a dust-poor quasar and a dusty, potentially gas-rich starburst galaxy.

To investigate this system we carried out CO(1-0) observations using VLA. We detect bright CO(1-0) emission associated with the quasar and an additional CO component (hereafter referred to as companion) at $\sim 2.3''$ ($\sim$ 17 kpc) projected distance from the quasar. The companion is also shifted by $\sim 800\,\mathrm{km\,s^{-1}}$ in velocity with respect to the optical redshift of the quasar. The peak of the submm emission is not coincident with the position of the CO companion, there is a projected separation of $\sim 1.4''$ between them. On the one hand the observed offset between the submm peak and the CO companion could be related to the resolution of the VLA observations ($\sim 3''$), which is lower compared to the SMA observation. In addition, observational errors can affect the astrometric accuracy of the VLA data. On the other hand, such offsets has been observed in other low- and high-redshift sources.

For instance, a very similar scenario is seen in Arp 244 (a.k.a. the Antennae galaxies), where the two merging galaxies have significant CO(1–0) emission and a dusty, gas-rich overlap region is observed between them. This overlap region is the most luminous component in the mid-IR, and is associated with the highest star formation activity and dust temperature. A high-redshift analogue of SDSS 160705+533558 is the first discovered and spectroscopically confirmed submillimetre galaxy, SMM J02399-0136 ($z = 2.8$). This system consists of four components, including a BAL QSO, dusty starburst component, and two UV systems with modest stellar masses. It has been suggested, that the two merging galaxies are

the quasar and one of the UV components, with the dusty starburst being the overlap region, similar to Arp 244, where the star formation is triggered by the galaxy interaction. However, in the case of SMM J02399-0136, the majority of the CO emission is associated with the starburst component. In order to confirm the presence of the CO companion and disentangle the different components observed in this source, higher-resolution CO and submm observations are necessary.

My contribution to Paper IV
I selected the source, and was the PI of the VLA observations. I imaged the data and carried out the data analysis, and prepared the manuscript.

Chapter 7

Outlook and future prospects

Studies of high-z quasars and HzRGs and their environment indicate that these AGN might be signposts of overdense regions in the Universe, surrounded by submm galaxies and often associated with close gas-rich, star-forming companions. In this thesis I presented three case studies of high-z AGNs, which were selected based on having a gas-rich and/or submm-bright companion, while the host galaxies of the AGNs appeared gas-poor. Follow-up, sensitive and high-resolution observations with ALMA and VLA, tracing CO line emission and dust continuum emission revealed that a significant amount of molecular gas and dust emission is associated with the host galaxies of the AGNs. These results demonstrate that we are on the right track to understand the evolution of massive, elliptical galaxies.

However, one of the biggest limiting factor of high-z studies is angular resolution. To date, the largest far-infared surveys of quasars have been perfomed with e.g. the *Herschel Space Observatory* or SCUBA(-2) at the JCMT but these observations do not provide sufficient spatial resolution to resolve FIR emission and to pinpoint its exact origin (e.g. SCUBA beam is 15" at 850 μm, *Herschel* SPIRE beam at 250 μm is $\sim$ 18"). These surveys revealed several quasars with very high FIR luminosities indicating high SFR in their host galaxies. The question is whether they are indeed going through a starburst and reaching their maximum SFR or the FIR emission comes from multiple galaxies blended in a large beam. Both scenarios are possible: e.g. Wang et al. (2013) measured the dust continuum of $z = 6$ quasars with ALMA and their measurements indicate vigorous star formation over the central region in the quasar host galaxies, while Emonts et al. (2015) concluded that one the most IR luminous HzRG MRC0152-209 is in fact a triple merger system and the high IR emission is the result of intense star formation in each galaxy component.

The strength of submm interferometers has been demonstrated in case of high-z SMGs, where a fraction of SMGs resolved into multiple distinct sources compared to large beam observations (e.g. Wang et al. 2011; Smolčić et al. 2012; Barger et al.

2012; Hodge et al. 2013; Karim et al. 2013). Therefore, it is possible that *Herschel* detected FIR-bright quasars might have unresolved companion galaxies and thus the use of high-resolution observations is essential. In addition to submm studies, we can use other tracers to characterise the environment of high-z AGN, such as CO transition lines to determine the properties of the molecular gas (physical conditions, mass) and for kinematic studies or the optically thin [C II] cooling line, which can be used to estimate SFR, even in case of obscured galaxies. Using emission lines has the advantage of providing redshift information, which many earlier studies lacked.

In addition to sensitive, high-resolution studies of high-z AGNs, tracing star-formation and molecular gas at small scales, we need to extend protocluster studies to even larger scales to get a complete picture of galaxy evolution and cover all the bases. As protoclusters are very extended, previous observations only covered small parts of them, typically the largest halo of the protocluster (Muldrew et al. 2015). However, to study the evolution of cluster galaxies it is crucial to observe a large fraction of the protocluster, not only its core. Thus observations spanning several arcmin are necessary to uncover all the physical processes that shape the evolution of clusters and their members. The ultimate goal is to link the small-scale observational findings to that of large-scale protocluster studies and see what relations emerge from it.

Bibliography

Aalto, S., Garcia-Burillo, S., Muller, S., et al. 2012, A&A, 537, A44

Adams, S. M., Martini, P., Croxall, K. V., Overzier, R. A., & Silverman, J. D. 2015, MNRAS, 448, 1335

Aird, J., Nandra, K., Laird, E. S., et al. 2010, MNRAS, 401, 2531

Antonucci, R. 1993, ARA&A, 31, 473

Aragon Calvo, M. A., Neyrinck, M. C., & Silk, J. 2019, The Open Journal of Astrophysics, 2, 7

Banerji, M., Carilli, C. L., Jones, G., et al. 2017, MNRAS, 465, 4390

Barger, A. J., Wang, W.-H., Cowie, L. L., et al. 2012, ApJ, 761, 89

Barthel, P. D. 1989, ApJ, 336, 606

Baugh, C. M. 2006, Reports on Progress in Physics, 69, 3101

Best, P. N. 2000, MNRAS, 317, 720

Best, P. N., Lehnert, M. D., Miley, G. K., & Röttgering, H. J. A. 2003, MNRAS, 343, 1

Best, P. N., Longair, M. S., & Roettgering, H. J. A. 1998, MNRAS, 295, 549

Bigiel, F., Leroy, A., Walter, F., et al. 2008, AJ, 136, 2846

Blain, A. W., Smail, I., Ivison, R. J., Kneib, J.-P., & Frayer, D. T. 2002, Phys. Rep., 369, 111

Blumenthal, G. R., Faber, S. M., Primack, J. R., & Rees, M. J. 1984, Nature, 311, 517

Boehringer, H., Voges, W., Fabian, A. C., Edge, A. C., & Neumann, D. M. 1993, MNRAS, 264, L25

Bohlin, R. C., Savage, B. D., & Drake, J. F. 1978, ApJ, 224, 132

Bolatto, A. D., Wolfire, M., & Leroy, A. K. 2013, ARA&A, 51, 207

Borisova, E., Cantalupo, S., Lilly, S. J., et al. 2016, ApJ, 831, 39

Bothwell, M. S., Smail, I., Chapman, S. C., et al. 2013, MNRAS, 429, 3047

Bouwens, R. J., Illingworth, G. D., Franx, M., & Ford, H. 2007, ApJ, 670, 928

Bruzual, G. & Charlot, S. 2003, MNRAS, 344, 1000

Cantalupo, S., Arrigoni-Battaia, F., Prochaska, J. X., Hennawi, J. F., & Madau, P. 2014, Nature, 506, 63

Cantalupo, S., Porciani, C., Lilly, S. J., & Miniati, F. 2005, ApJ, 628, 61

Cappellari, M., McDermid, R. M., Alatalo, K., et al. 2013, MNRAS, 432, 1862

Cardelli, J. A., Clayton, G. C., & Mathis, J. S. 1989, ApJ, 345, 245

Carilli, C. L., Röttgering, H. J. A., van Ojik, R., Miley, G. K., & van Breugel, W. J. M. 1997, ApJS, 109, 1

Carilli, C. L. & Walter, F. 2013, ARA&A, 51, 105

Carniani, S., Marconi, A., Maiolino, R., et al. 2017, A&A, 605, A105

Casey, C. M., Narayanan, D., & Cooray, A. 2014, Phys. Rep., 541, 45

Caucci, S., Colombi, S., Pichon, C., et al. 2008, MNRAS, 386, 211

Chabrier, G. 2003, PASP, 115, 763

Champagne, J. B., Decarli, R., Casey, C. M., et al. 2018, ApJ, 867, 153

Charlot, S. & Fall, S. M. 2000, ApJ, 539, 718

Chary, R. & Elbaz, D. 2001, ApJ, 556, 562

Chiang, Y.-K., Overzier, R., & Gebhardt, K. 2013, ApJ, 779, 127

Clements, D. L., Petitpas, G., Farrah, D., et al. 2009, ApJ, 698, L188

Cole, S., Benson, A., Baugh, C., Lacey, C., & Frenk, C. 2000a, in Astronomical Society of the Pacific Conference Series, Vol. 200, Clustering at High Redshift, ed. A. Mazure, O. Le Fèvre, & V. Le Brun, 109

Cole, S., Lacey, C. G., Baugh, C. M., & Frenk, C. S. 2000b, MNRAS, 319, 168

Condon, J. J. & Ransom, S. M. 2016, Essential Radio Astronomy

Conroy, C. 2013, ARA&A, 51, 393

Cooke, E. A., Hatch, N. A., Muldrew, S. I., Rigby, E. E., & Kurk, J. D. 2014, MNRAS, 440, 3262

Croft, S., Kurk, J., van Breugel, W., et al. 2005, AJ, 130, 867

da Cunha, E., Charlot, S., & Elbaz, D. 2008, MNRAS, 388, 1595

da Cunha, E., Groves, B., Walter, F., et al. 2013, ApJ, 766, 13

da Cunha, E., Walter, F., Smail, I. R., et al. 2015, ApJ, 806, 110

Daddi, E., Bournaud, F., Walter, F., et al. 2010, ApJ, 713, 686

Daddi, E., Cimatti, A., Renzini, A., et al. 2004, ApJ, 617, 746

Dale, D. A., Helou, G., Contursi, A., Silbermann, N. A., & Kolhatkar, S. 2001, ApJ, 549, 215

Dannerbauer, H., Lehnert, M. D., Lutz, D., et al. 2004, ApJ, 606, 664

Davis, M., Efstathiou, G., Frenk, C. S., & White, S. D. M. 1985, ApJ, 292, 371

De Breuck, C., Downes, D., Neri, R., et al. 2005, A&A, 430, L1

Decarli, R., Walter, F., Venemans, B. P., et al. 2017, Nature, 545, 457

Dekel, A. & Birnboim, Y. 2006, MNRAS, 368, 2

Dekel, A., Birnboim, Y., Engel, G., et al. 2009a, Nature, 457, 451

Dekel, A., Sari, R., & Ceverino, D. 2009b, ApJ, 703, 785

Dickman, R. L., Snell, R. L., & Schloerb, F. P. 1986, ApJ, 309, 326

Donoso, E., Li, C., Kauffmann, G., Best, P. N., & Heckman, T. M. 2010, MNRAS, 407, 1078

Downes, D. & Solomon, P. M. 1998, ApJ, 507, 615

Draine, B. T. 2003, ARA&A, 41, 241

Draine, B. T. 2011, Physics of the Interstellar and Intergalactic Medium

Draine, B. T. & Li, A. 2007, ApJ, 657, 810

Dressler, A. 1980, ApJ, 236, 351

Drouart, G. & Falkendal, T. 2018, Monthly Notices of the Royal Astronomical Society, 477, 4981

Dunn, R. J. H. & Fabian, A. C. 2006, MNRAS, 373, 959

Dunn, R. J. H. & Fabian, A. C. 2008, MNRAS, 385, 757

Eckart, A. & Genzel, R. 1996, Nature, 383, 415

Elston, R., Rieke, G. H., & Rieke, M. J. 1988, ApJ, 331, L77

Emonts, B. H. C., De Breuck, C., Lehnert, M. D., et al. 2015, A&A, 584, A99

Faber, S. M., Willmer, C. N. A., Wolf, C., et al. 2007, ApJ, 665, 265

Fabian, A. C. 2012, ARA&A, 50, 455

Falder, J. T., Stevens, J. A., Jarvis, M. J., et al. 2011, ApJ, 735, 123

Fall, S. M. & Efstathiou, G. 1980, MNRAS, 193, 189

Fanaroff, B. L. & Riley, J. M. 1974, MNRAS, 167, 31P

Fanidakis, N., Baugh, C. M., Benson, A. J., et al. 2011a, MNRAS, 410, 53

Fanidakis, N., Baugh, C. M., Benson, A. J., et al. 2011b, MNRAS, 410, 53

Fanidakis, N., Baugh, C. M., Benson, A. J., et al. 2012, MNRAS, 419, 2797

Fanidakis, N., Macciò, A. V., Baugh, C. M., Lacey, C. G., & Frenk, C. S. 2013, MNRAS, 436, 315

Feruglio, C., Maiolino, R., Piconcelli, E., et al. 2010, A&A, 518, L155

Franx, M., Labbé, I., Rudnick, G., et al. 2003, ApJ, 587, L79

Fumagalli, M., Prochaska, J. X., Kasen, D., et al. 2011, MNRAS, 418, 1796

Galametz, A., Stern, D., De Breuck, C., et al. 2012, ApJ, 749, 169

Galametz, A., Stern, D., Pentericci, L., et al. 2013, A&A, 559, A2

Galametz, A., Stern, D., Stanford, S. A., et al. 2010, A&A, 516, A101

Gebhardt, K., Bender, R., Bower, G., et al. 2000, ApJ, 539, L13

Genzel, R., Pichon, C., Eckart, A., Gerhard, O. E., & Ott, T. 2000, MNRAS, 317, 348

Genzel, R., Tacconi, L. J., Gracia-Carpio, J., et al. 2010, MNRAS, 407, 2091

Ghaffari, Z., Westhues, C., Haas, M., et al. 2017, Astronomische Nachrichten, 338, 823

Ghez, A. M., Klein, B. L., Morris, M., & Becklin, E. E. 1998, ApJ, 509, 678

Gonzalez-Perez, V., Lacey, C. G., Baugh, C. M., et al. 2014, MNRAS, 439, 264

Greene, J. E., Zakamska, N. L., & Smith, P. S. 2012, ApJ, 746, 86

Greve, T. R., Stern, D., Ivison, R. J., et al. 2007, MNRAS, 382, 48

Gullberg, B., De Breuck, C., Lehnert, M. D., et al. 2016, A&A, 586, A124

Häring, N. & Rix, H.-W. 2004, ApJ, 604, L89

Hatch, N. A., Kurk, J. D., Pentericci, L., et al. 2011, MNRAS, 415, 2993

Hatch, N. A., Wylezalek, D., Kurk, J. D., et al. 2014, MNRAS, 445, 280

Hatziminaoglou, E., Pérez-Fournon, I., Polletta, M., et al. 2005, AJ, 129, 1198

Heckman, T. M. & Best, P. N. 2014, ARA&A, 52, 589

Hill, G. J. & Lilly, S. J. 1991, ApJ, 367, 1

Hodge, J. A., Karim, A., Smail, I., et al. 2013, ApJ, 768, 91

Hopkins, A. M. 2004, ApJ, 615, 209

Hopkins, P. F., Hernquist, L., Cox, T. J., et al. 2006, ApJS, 163, 1

Hopkins, P. F., Hernquist, L., Cox, T. J., & Kereš, D. 2008, ApJS, 175, 356

Hughes, D. H., Serjeant, S., Dunlop, J., et al. 1998, Nature, 394, 241

Husband, K., Bremer, M. N., Stanway, E. R., & Lehnert, M. D. 2015, MNRAS, 452, 2388

Husband, K., Bremer, M. N., Stott, J. P., & Murphy, D. N. A. 2016, MNRAS, 462, 421

Ivison, R. J., Dunlop, J. S., Smail, I., et al. 2000, ApJ, 542, 27

Ivison, R. J., Morrison, G. E., Biggs, A. D., et al. 2008, MNRAS, 390, 1117

Ivison, R. J., Papadopoulos, P. P., Smail, I., et al. 2011, MNRAS, 412, 1913

Ivison, R. J., Smail, I., Amblard, A., et al. 2012, MNRAS, 425, 1320

Izquierdo-Villalba, D., Orsi, Á. A., Bonoli, S., et al. 2018, MNRAS, 480, 1340

Jones, S. F., Blain, A. W., Lonsdale, C., et al. 2015, MNRAS, 448, 3325

Karim, A., Swinbank, A. M., Hodge, J. A., et al. 2013, MNRAS, 432, 2

Katz, N., Keres, D., Dave, R., & Weinberg, D. H. 2003, in Astrophysics and Space Science Library, Vol. 281, The IGM/Galaxy Connection. The Distribution of Baryons at z=0, ed. J. L. Rosenberg & M. E. Putman, 185

Kennicutt, Robert C., J. 1998, ApJ, 498, 541

Kereš, D., Katz, N., Weinberg, D. H., & Davé, R. 2005, MNRAS, 363, 2

Knudsen, K. K., van der Werf, P. P., & Jaffe, W. 2003, A&A, 411, 343

Komatsu, E., Smith, K. M., Dunkley, J., et al. 2011, ApJS, 192, 18

Kormendy, J., Fisher, D. B., Cornell, M. E., & Bender, R. 2009, ApJS, 182, 216

Kormendy, J. & Ho, L. C. 2013, ARA&A, 51, 511

Kormendy, J. & Kennicutt, Robert C., J. 2004, ARA&A, 42, 603

Kormendy, J. & Richstone, D. 1995, ARA&A, 33, 581

Kroupa, P. 2002, Science, 295, 82

Kurk, J. D., Pentericci, L., Overzier, R. A., Röttgering, H. J. A., & Miley, G. K. 2004a, A&A, 428, 817

Kurk, J. D., Pentericci, L., Röttgering, H. J. A., & Miley, G. K. 2004b, A&A, 428, 793

Kurk, J. D., Röttgering, H. J. A., Pentericci, L., et al. 2000, A&A, 358, L1

Lagos, C. d. P., Bayet, E., Baugh, C. M., et al. 2012, MNRAS, 426, 2142

Lanz, L., Zezas, A., Brassington, N., et al. 2013, ApJ, 768, 90

Le Fevre, O., Deltorn, J. M., Crampton, D., & Dickinson, M. 1996, ApJ, 471, L11

Lee, K.-G., Hennawi, J. F., White, M., et al. 2016, ApJ, 817, 160

Lee, K.-G. & White, M. 2016, ApJ, 831, 181

Leroy, A. K., Walter, F., Brinks, E., et al. 2008, AJ, 136, 2782

Li, Q., Narayanan, D., & Davé, R. 2019, MNRAS, 490, 1425

Lin, L., Cooper, M. C., Jian, H.-Y., et al. 2010, ApJ, 718, 1158

Lonsdale, C., Polletta, M. d. C., Surace, J., et al. 2004, ApJS, 154, 54

Madau, P. & Dickinson, M. 2014, ARA&A, 52, 415

Magliocchetti, M., Popesso, P., Brusa, M., & Salvato, M. 2018, MNRAS, 478, 3848

Magorrian, J., Tremaine, S., Richstone, D., et al. 1998, AJ, 115, 2285

Marconi, A. & Hunt, L. K. 2003, ApJ, 589, L21

Martin, D. C., Matuszewski, M., Morrissey, P., et al. 2015, Nature, 524, 192

Mazzucchelli, C., Bañados, E., Decarli, R., et al. 2017, ApJ, 834, 83

McConnell, N. J. & Ma, C.-P. 2013, ApJ, 764, 184

McNamara, B. R., Wise, M., Nulsen, P. E. J., et al. 2000, ApJ, 534, L135

Merritt, D. & Ferrarese, L. 2001, MNRAS, 320, L30

Morganti, R., Holt, J., Saripalli, L., Oosterloo, T. A., & Tadhunter, C. N. 2007, A&A, 476, 735

Muldrew, S. I., Hatch, N. A., & Cooke, E. A. 2015, MNRAS, 452, 2528

Nelson, D., Genel, S., Vogelsberger, M., et al. 2015, MNRAS, 448, 59

Nesvadba, N. P. H., Neri, R., De Breuck, C., et al. 2009, MNRAS, 395, L16

Nesvadba, N. P. H., Polletta, M., Lehnert, M. D., et al. 2011, MNRAS, 415, 2359

Netzer, H. 2015, ARA&A, 53, 365

Orsi, Á. A., Fanidakis, N., Lacey, C. G., & Baugh, C. M. 2016, MNRAS, 456, 3827

Overzier, R. A. 2016, A&A Rev., 24, 14

Partridge, R. B. & Peebles, P. J. E. 1967, ApJ, 147, 868

Pentericci, L., Kurk, J. D., Röttgering, H. J. A., et al. 2000, A&A, 361, L25

Pentericci, L., Röttgering, H. J. A., Miley, G. K., et al. 1999, A&A, 341, 329

Pope, A., Scott, D., Dickinson, M., et al. 2006, MNRAS, 370, 1185

Priddey, R. S., Ivison, R. J., & Isaak, K. G. 2008, MNRAS, 383, 289

Prochaska, J. X. & Hennawi, J. F. 2009, ApJ, 690, 1558

Rachford, B. L., Snow, T. P., Destree, J. D., et al. 2009, ApJS, 180, 125

Rees, M. J. & Ostriker, J. P. 1977, MNRAS, 179, 541

Rémy-Ruyer, A., Madden, S. C., Galliano, F., et al. 2014, A&A, 563, A31

Renzini, A. 1999, in The Formation of Galactic Bulges, ed. C. M. Carollo, H. C. Ferguson, & R. F. G. Wyse, 9

Richstone, D., Ajhar, E. A., Bender, R., et al. 1998, Nature, 395, A14

Riechers, D. A. 2013, ApJ, 765, L31

Riechers, D. A., Walter, F., Bertoldi, F., et al. 2009, ApJ, 703, 1338

Riechers, D. A., Walter, F., Carilli, C. L., Bertoldi, F., & Momjian, E. 2008, ApJ, 686, L9

Riechers, D. A., Walter, F., Carilli, C. L., et al. 2006, ApJ, 650, 604

Rigby, E. E., Hatch, N. A., Röttgering, H. J. A., et al. 2014, MNRAS, 437, 1882

Roettgering, H. J. A., Lacy, M., Miley, G. K., Chambers, K. C., & Saunders, R. 1994, A&AS, 108, 79

Rosdahl, J. & Blaizot, J. 2012, MNRAS, 423, 344

Rowlands, K., Dunne, L., Dye, S., et al. 2014, MNRAS, 441, 1017

Rupke, D. S. N. & Veilleux, S. 2013, ApJ, 775, L15

Salomé, P., Guélin, M., Downes, D., et al. 2012, A&A, 545, A57

Salpeter, E. E. 1955, ApJ, 121, 161

Sanders, D. B. & Mirabel, I. F. 1996, ARA&A, 34, 749

Savage, B. D. & Mathis, J. S. 1979, ARA&A, 17, 73

Schmidt, M. 1959, ApJ, 129, 243

Schruba, A., Leroy, A. K., Walter, F., et al. 2011, AJ, 142, 37

Seymour, N., Stern, D., De Breuck, C., et al. 2007, ApJS, 171, 353

Shen, Y., Strauss, M. A., Ross, N. P., et al. 2009, ApJ, 697, 1656

Shlosman, I. 2013, Cosmological Evolution of Galaxies, ed. J. Falcón-Barroso & J. H. Knapen, 555

Siebenmorgen, R. & Krügel, E. 2007, A&A, 461, 445

Silk, J. 1977, ApJ, 211, 638

Silva, A., Sajina, A., Lonsdale, C., & Lacy, M. 2015, ApJ, 806, L25

Silva, L., Granato, G. L., Bressan, A., & Danese, L. 1998, ApJ, 509, 103

Smail, I., Ivison, R. J., & Blain, A. W. 1997, ApJ, 490, L5

Smolčić, V., Aravena, M., Navarrete, F., et al. 2012, A&A, 548, A4

Smolčić, V., Karim, A., Miettinen, O., et al. 2015, A&A, 576, A127

Solomon, P. M. & Barrett, J. W. 1991, in IAU Symposium, Vol. 146, Dynamics of Galaxies and Their Molecular Cloud Distributions, ed. F. Combes & F. Casoli, 235

Solomon, P. M., Downes, D., & Radford, S. J. E. 1992, ApJ, 398, L29

Solomon, P. M., Rivolo, A. R., Barrett, J., & Yahil, A. 1987, ApJ, 319, 730

Soltan, A. 1982, MNRAS, 200, 115

Springel, V., White, S. D. M., Jenkins, A., et al. 2005, Nature, 435, 629

Stark, C. W., Font-Ribera, A., White, M., & Lee, K.-G. 2015, MNRAS, 453, 4311

Steidel, C. C., Pettini, M., & Hamilton, D. 1995, AJ, 110, 2519

Stevens, J. A., Ivison, R. J., Dunlop, J. S., et al. 2003, Nature, 425, 264

Stevens, J. A., Jarvis, M. J., Coppin, K. E. K., et al. 2010, MNRAS, 405, 2623

Stevens, J. A., Page, M. J., Ivison, R. J., Smail, I., & Carrera, F. J. 2004, ApJ, 604, L17

Swinbank, A. M., Vernet, J. D. R., Smail, I., et al. 2015, MNRAS, 449, 1298

Tacconi, L. J., Genzel, R., Smail, I., et al. 2008, ApJ, 680, 246

Tadhunter, C. 2008, New A Rev., 52, 227

Taylor, G. B., Carilli, C. L., & Perley, R. A. 1999, Synthesis Imaging in Radio Astronomy II, Vol. 180

Trakhtenbrot, B., Lira, P., Netzer, H., et al. 2017, ApJ, 836, 8

Tremaine, S., Gebhardt, K., Bender, R., et al. 2002, ApJ, 574, 740

Trump, J. R., Hall, P. B., Reichard, T. A., et al. 2006, ApJS, 165, 1

Trumpler, R. J. 1930, PASP, 42, 214

Uchiyama, H., Toshikawa, J., Kashikawa, N., et al. 2018, PASJ, 70, S32

Umehata, H., Fumagalli, M., Smail, I., et al. 2019, Science, 366, 97

Urry, C. M. & Padovani, P. 1995, PASP, 107, 803

van de Voort, F., Bahé, Y. M., Bower, R. G., et al. 2017, MNRAS, 466, 3460

van de Voort, F., Schaye, J., Booth, C. M., & Dalla Vecchia, C. 2011a, MNRAS, 415, 2782

van de Voort, F., Schaye, J., Booth, C. M., Haas, M. R., & Dalla Vecchia, C. 2011b, MNRAS, 414, 2458

van der Tak, F. F. S., Black, J. H., Schöier, F. L., Jansen, D. J., & van Dishoeck, E. F. 2007, A&A, 468, 627

Venemans, B. P., Röttgering, H. J. A., Miley, G. K., et al. 2007, A&A, 461, 823

Vernet, J., Lehnert, M. D., De Breuck, C., et al. 2017, A&A, 602, L6

Vikhlinin, A. A., Kravtsov, A. V., Markevich, M. L., Sunyaev, R. A., & Churazov, E. M. 2014, Physics Uspekhi, 57, 317

Vogelsberger, M., Genel, S., Springel, V., et al. 2014, Nature, 509, 177

Walter, F., Weiss, A., & Scoville, N. 2002, ApJ, 580, L21

Wang, R., Wagg, J., Carilli, C. L., et al. 2013, ApJ, 773, 44

Wang, W.-H., Cowie, L. L., Barger, A. J., & Williams, J. P. 2011, ApJ, 726, L18

White, S. D. M. & Frenk, C. S. 1991, ApJ, 379, 52

White, S. D. M. & Rees, M. J. 1978, MNRAS, 183, 341

Wilson, T. L., Rohlfs, K., & Hüttemeister, S. 2009, Tools of Radio Astronomy

Wong, T. & Blitz, L. 2002, ApJ, 569, 157

Wylezalek, D., Galametz, A., Stern, D., et al. 2013, ApJ, 769, 79

Wylezalek, D., Vernet, J., De Breuck, C., et al. 2014, ApJ, 786, 17

Yates, M. G., Miller, L., & Peacock, J. A. 1989, MNRAS, 240, 129

Zubko, V., Dwek, E., & Arendt, R. G. 2004, ApJS, 152, 211